AERONAUTICS INSTITUTE OF TECHNOLOGY

Felipe Mello dos Reis

DEVELOPMENT OF ONE-PART ALKALI-ACTIVATED CEMENT WITH LOW-CALCIUM SOLID PRECURSORS AND ALTERNATIVE ALKALINE SOURCES.

Final Paper
2025

Course of Civil-Aeronautics Engineering

CDU 624:666.94

Felipe Mello dos Reis

DEVELOPMENT OF ONE-PART ALKALI-ACTIVATED CEMENT WITH LOW-CALCIUM SOLID PRECURSORS AND ALTERNATIVE ALKALINE SOURCES.

Advisor

Prof. Dr. João Cláudio Bassan de Moraes (ITA)

CIVIL-AERONAUTICS ENGINEERING

São José dos Campos
Aeronautics Institute of Technology

2025

Cataloging-in Publication Data
Documentation and Information Division

dos Reis, Felipe Mello
Development of one-part alkali-activated cement with low-calcium solid precursors and alternative alkaline sources. / Felipe Mello dos Reis.
São José dos Campos, 2025.
57f.

Final paper (Undergraduation study) – Course of Civil-Aeronautics Engineering– Instituto Tecnológico de Aeronáutica, 2025. Advisor: Prof. Dr. João Cláudio Bassan de Moraes.

1. Alkali activated material. 2. Geopolymer. 3. One-part. I. Instituto Tecnológico de Aeronáutica. II. Title.

BIBLIOGRAPHIC REFERENCE

DOS REIS, Felipe Mello. **Development of one-part alkali-activated cement with low-calcium solid precursors and alternative alkaline sources.**. 2025. 57f. Final paper (Undergraduation study) – Instituto Tecnológico de Aeronáutica, São José dos Campos.

CESSION OF RIGHTS

Felipe Mello dos Reis
Rua H8A, Ap. 113
12.228-460 – São José dos Campos–SP

DEVELOPMENT OF ONE-PART ALKALI-ACTIVATED CEMENT WITH LOW-CALCIUM SOLID PRECURSORS AND ALTERNATIVE ALKALINE SOURCES.

Final Work approved in its final version by signatories below:

Documento assinado digitalmente
gov.br
FELIPE MELLO DOS REIS
Data: 20/11/2025 10:23:22-0300
Verifique em https://validar.iti.gov.br

Felipe Mello dos Reis

Author

Documento assinado digitalmente
gov.br
JOAO CLAUDIO BASSAN DE MORAES
Data: 20/11/2025 10:44:41-0300
Verifique em https://validar.iti.gov.br

João Cláudio Bassan de Moraes (ITA)

Advisor

São José dos Campos: November 12, 2025.

I dedicate this work to all those who believed in my dream of graduating from the Aeronautics Institute of Technology and helped me make it a reality.

Acknowledgments

Primeiramente, gostaria de agradecer a Deus, pois só cheguei até aqui graças a Ele.

Ao meu orientador, Prof. Dr. João Cláudio Bassan de Moraes, pela confiança e pelos desafios propostos, que foram essenciais para o meu crescimento acadêmico e pessoal durante a realização deste trabalho.

Aos meus colegas de H8, especialmente João Pedro, Spirandelli, João Victor, Aluísio, Carol, Hermiro e Robalinho, que se tornaram parte da minha família nesses anos de curso. De todos os momentos compartilhados, desde os de descontração até as horas da madrugada estudando juntos, levo comigo amizades que certamente durarão para a vida toda.

À minha namorada, Clara, pelo carinho, paciência e por estar sempre ao meu lado. Não houve distância ou obstáculo que pudesse abalar nosso relacionamento durante essa jornada.

À minha irmã, Fernanda, por ser a minha primeira e melhor amiga, minha fortaleza em todos os momentos. Sem dúvida, foi a sua confiança no meu potencial que me fez elevar o nível e voar mais alto.

Por fim, devo agradecer àqueles sem os quais nem o início dessa caminhada seria possível: meus pais. Vocês são minha base e inspiração; reconheço que, sem os valores ensinados, o amor incondicional e os sacrifícios de vocês, eu não estaria aqui hoje. Essa vitória é de vocês e por vocês.

"For everyone to whom much is given, from him much will be required; and to whom much has been committed, of him they will ask the more. "
— Luke 12:48

Resumo

Na busca por alternativas mais sustentáveis ao cimento Portland, os cimentos ativados alcalinamente têm sido amplamente estudados. Inicialmente, a maioria dos processos de mistura ocorre em duas etapas, que sacrificam a eficiência produtiva em favor de melhores propriedades mecânicas. Visando aumentar a escalabilidade do processo, o desenvolvimento de sistemas monocomponentes ("just-add-water") trouxe uma tecnologia mais acessível e prática para a indústria. No entanto, os estudos atuais se concentram principalmente em precursores ricos em cálcio, enquanto o uso de ativadores alcalinos convencionais levanta preocupações relacionadas à segurança e ao impacto ambiental. Este trabalho propõe o desenvolvimento de um cimento ativado alcalinamente monocomponente usando precursores sólidos de baixo teor de cálcio, como sílica ativa e metacaulim, juntamente com fontes alcalinas mais seguras e sustentáveis, como carbonato de potássio e hidróxido de cálcio. A variação da razão molar Si/Al influenciou diretamente tanto a cinética de polimerização quanto as características microestruturais dos aglomerantes. Misturas com Si/Al = 3,0 alcançaram o melhor equilíbrio entre densidade, porosidade e resistência mecânica, refletindo um grau ótimo de geopolimerização e formação homogênea de gel. As análises microestruturais confirmaram a formação de géis aluminossilicatos predominantemente amorfos (K-A-S-H), com características do gel dependentes das proporções dos precursores. Os resultados demonstraram que a formulação proposta é tecnicamente viável, produzindo matrizes estáveis e compactas com desempenho mecânico adequado e maior segurança e sustentabilidade em comparação com sistemas ativados alcalinamente convencionais. O estudo demonstra que a combinação de metacaulim e sílica ativa com fontes alcalinas suaves é uma estratégia promissora para desenvolver um aglomerante com desempenho mecânico adequado e viabilidade aprimorada para aplicação na indústria da construção.

Abstract

In the search for more sustainable alternatives to Portland cement, alkali-activated cements have been extensively studied. Initially, most mixing processes occur in two steps, which sacrifice productive efficiency in favor of improved mechanical properties. Aiming to increase process scalability, the development of one-part (just-add-water) systems has brought a more accessible and practical technology to the industry. Nonetheless, current studies mainly focus on calcium-rich precursors, while the use of conventional alkaline activators raises concerns related to safety and environmental impact. This work proposes the development of a one-part alkali-activated cement using low-calcium solid precursors, such as silica fume and metakaolin, along with safer and sustainable alkaline sources, such as potassium carbonate and calcium hydroxide. The variation of the Si/Al molar ratio directly influenced both the polymerization kinetics and microstructural characteristics of the binders. Mixtures with Si/Al = 3.0 achieved the best balance between density, porosity, and mechanical strength, reflecting an optimal degree of geopolymerization and homogeneous gel formation. Microstructural analyses confirmed the formation of predominantly amorphous aluminosilicate gels (K-A-S-H), with gel characteristics dependent on precursor proportions. The results demonstrated that the proposed formulation is technically viable, producing stable and compact matrices with adequate mechanical performance and improved safety and sustainability compared to conventional alkali-activated systems. The study demonstrates that combining metakaolin and silica fume with mild alkaline sources is a promising strategy for developing a binder with adequate mechanical performance and enhanced viability for application in the construction industry.

List of Figures

List of Tables

List of Abbreviations and Acronyms

CO_2	carbon dioxide
GHG	greenhouse gases
SCM	supplementary cementitious materials
AAB	alkali-activated binder
AAM	alkali-activated material
AACB	alkali-activated concrete/binder
SiO_2	silica
Al_2O_3	alumina
N-A-S-H	sodium aluminate silicate hydrate
C-A-S-H	calcium aluminate silicate hydrate
K_2CO_3	potassium carbonate
$Ca(OH)_2$	calcium hydroxide
MK	metakaolin
SF	silica fume
FA	fly ash
CH	calcium hydroxide
KC	potassium carbonate
IPT	Institute for Technological Research
ITA	Aeronautics Institute of Technology
EDS	Energy dispersive X-ray spectroscopy
XRD	X-ray diffraction
OH^-	hydroxyl
FTIR	Fourier transform infrared spectroscopy
ABNT	Brazilian Association of Technical Standards
NBR	Brazilian Standard
ASTM	American Society for Testing and Materials
OPC	Ordinary Portland Cement
GGBFS	Ground Granulated Blast Furnace Slag
BFS	Blast Furnace Slag

MSWIA	Municipal Solid Waste Incineration Ash
NaOH	sodium hydroxide
Na_2SiO_3	sodium silicate
KOH	potassium hydroxide
Na_2CO_3	sodium carbonate
PSD	particle size distribution
LOI	loss on ignition
MIP	mercury intrusion porosimetry
IPT	Institute for Technological Research

Contents

1 Introduction

Portland cement is one of the main materials in civil construction, being used from the construction of houses and buildings to bridges and highways. In developing countries such as Brazil, cement is widely used due to its low complexity and cost, which allows its use on a large scale in any location. The exponential increase in cement production, having more than 30-fold since 1950 and almost 4-fold since 1990 (KELLY; MATOS, 2016), has been accompanied by a significant share of greenhouse gas (GHG) emissions, due to the calcination process of limestone that transforms calcium carbonate into calcium oxide and carbon dioxide in high-temperature furnaces. The production of Portland cement generates on average 842 kg of CO_2/t of clinker produced (ANDREW, 2018), representing 5.6% of anthropogenic GHG emissions (QUÉRÉ *et al.*, 2018).

In this context, there is a need to develop new cementitious materials that present three main properties: low GHG emissions, low cost, and high strength/durability (SCRIVENER *et al.*, 2018). A promising approach involves the implementation of supplementary cementitious materials (SCMs) or the introduction of new types of cements such as alkali-activated materials (AAMs) which are produced by a mixture between a solid precursor and an alkali source. These materials can partially or totally replace ordinary Portland cement by incorporating industrial products rich in silica and alumina, such as metakaolin, silica fume, or fly ash, significantly reducing the environmental footprint while maintaining or even enhancing mechanical performance and durability.

There are two ways in which AAMs can be produced: by mixing the solid precursor with an alkaline solution activator or with a solid alkaline source and water. Traditional two-part formulations, which require liquid solutions such as sodium silicate or sodium hydroxide, achieve high mechanical performance but are difficult to handle and store safely. One-part binders, in contrast, only require the addition of water to trigger the activation reaction, significantly improving scalability, storage safety, and field applicability (PROVIS, 2018). This approach also reduces the environmental and economic burdens associated with one-part systems, while maintaining satisfactory mechanical and durability performance under optimized mix conditions.

Despite the progress in AAMs, most current research relies on conventional activators

- particularly silicates and sodium hydroxide (ZAREECHIAN *et al.*, 2023) - that pose environmental and safety challenges. The production of sodium silicate, for instance, emits about 1.2 kg of CO_2 per kg produced (NEUPANE, 2022) and requires temperatures above 1200-1400 °C (VINAI; SOUTSOS, 2019), while NaOH solutions are highly caustic and hazardous for large-scale handling. The substitution of these activators by solid, less aggressive alternatives such as potassium carbonate (K_2CO_3) or calcium hydroxide ($Ca(OH)_2$) can mitigate these issues by reducing energy demand, minimizing GHG emissions, and improving user safety.

Furthermore, calcium-rich precursors such as blast furnace slag and fly ash have dominated alkali-activation research due to several advantages, such as rapid strength development (PROVIS; BERNAL, 2014), reduced reliance on thermal curing (KE *et al.*, 2021), and the formation of denser and less porous matrices by C-A-S-H reaction products compared to K-A-S-H gels (BERNAL *et al.*, 2014). However, their availability is regionally limited and their chemistry often results in brittle matrices prone to shrinkage and cracking. Low-calcium precursors—such as metakaolin and silica fume—offer a broader, more sustainable alternative, forming amorphous K-A-S-H type gels with low permeability, high thermal stability, and reduced susceptibility to chemical attack.

Expandig the use of these materials is particularly relevant for one-part systems, as they can incorporate a wider variety of industrial by-products and natural minerals while maintaining durability and reducing environmental impact. In this sense, this work proposes the development of one-part alkali-activated cements using low-calcium solid precursors and alternative alkaline sources. This approach aims to contribute to the formulation of more sustainable, safe, and adequately performing binders for applications in civil construction, aligning with contemporary guidelines for low environmental impact (BRASIL, 2016).

2 Literature Review

2.1 Definition and Reaction Mechanism of Alkali-Activated Materials

Alkali-activated materials (AAMs) are a class of inorganic materials produced by the reaction of an aluminosilicate precursor with an alkaline source under controlled conditions, forming a hardened matrix similar or superior to ordinary Portland cement (OPC). Within this family, geopolymers represent a subclass characterized by low calcium content and the predominance of amorphous sodium or potassium aluminosilicate hydrate gels (N-A-S-H or C-A-S-H, respectively) (PROVIS, 2018). The distinction between them lies in both composition and reaction mechanisms, as depicted in Figure 2.1.

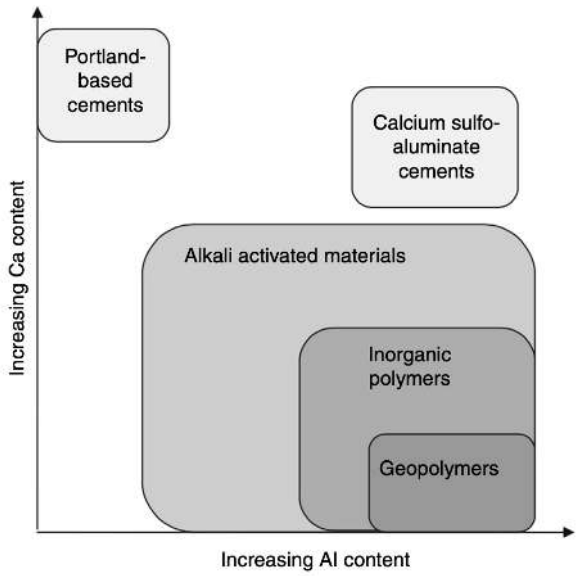

FIGURE 2.1 – Classification of different subsets of alkali-activated materials, with comparisons to Portland cement and calcium sulfoaluminate binder chemistry. Shading indicates approximate alkali content; darker shading corresponds to higher concentrations of Na and/or K (RAKHIMOVA; RAKHIMOV, 2019b).

The chemical mechanism involves three main stages: (i) dissolution of the aluminosilicate framework of the precursor under highly alkaline conditions, releasing silicate and aluminate species; (ii) reorganization and condensation of these dissolved species into chains;

and (iii) polycondensation forming a three-dimensional gel network that subsequently hardens into a solid binder (SEVERO *et al.*, 2013; DUXSON A. FERNÁNDEZ-JIMÉNEZ, 2006). Figure 2.2 illustrates this process.

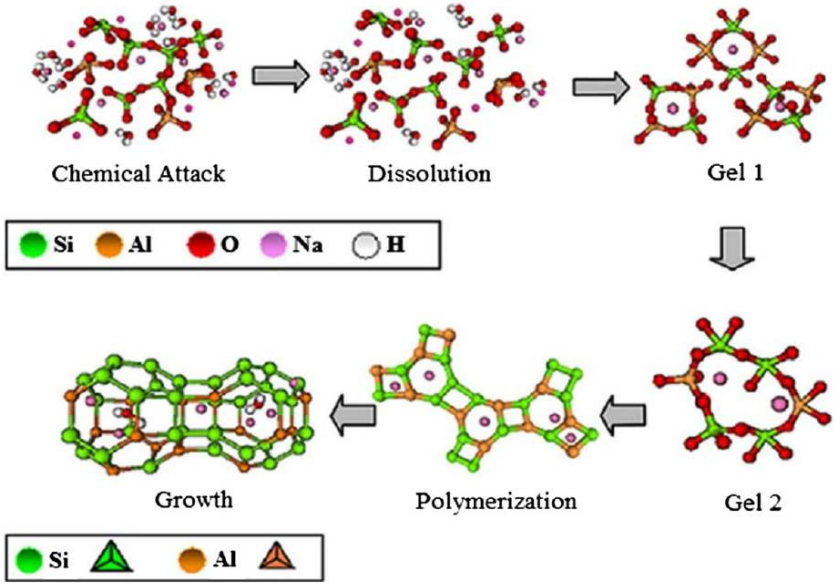

FIGURE 2.2 – Scheme of the alkaline activation process (DUXSON A. FERNÁNDEZ-JIMÉNEZ, 2006).

The resulting gel composition-typically N-A-S-H for low-calcium precursors and C-A-S-H for high-calcium precursors-depends on both the chemistry of the starting materials and the activation conditions.

2.2 Historical Context

The synthesis of materials by alkali activation began in the 1930s and 1940s, when a substitute for traditional Portland cement was developed from blast furnace slag and other aluminosilicates (PACHECO-TORGAL *et al.*, 2014). From the 1970s onwards, interest in this area increased, when the French scientist Joseph Davidovits coined the term "geopolymer" and patented several formulations. His initial studies focused on the development of inorganic, non-flammable, and fire-resistant materials (PROVIS; DEVENTER, 2009).

Since then, alkali-activated materials have attracted the attention of researchers and industry due to their low energy consumption and sustainable nature (QIN *et al.*, 2022). Furthermore, as studies have advanced, AAMs have gained recognition for their mechanical properties and durability, as the polymerization reactions that occur during curing provide high compressive strength and resistance to chemical attack.

2.3 Raw Materials for Alkali-Activated Systems

2.3.1 Precursors

Precursors are aluminosilicate-rich solids that react with alkaline activators to form polymeric gels. They are generally categorized into three main groups depending on their calcium oxide content and the dominant hydration products (LUUKKNEN Z. ABDOLLAHNEJAD, 2017; PACHECO-TORGAL *et al.*, 2014).

Figure 2.3 shows the most common precursors and their respective chemical compositions. For further details, Annex A presents their main characteristic, limitations, and benefits.

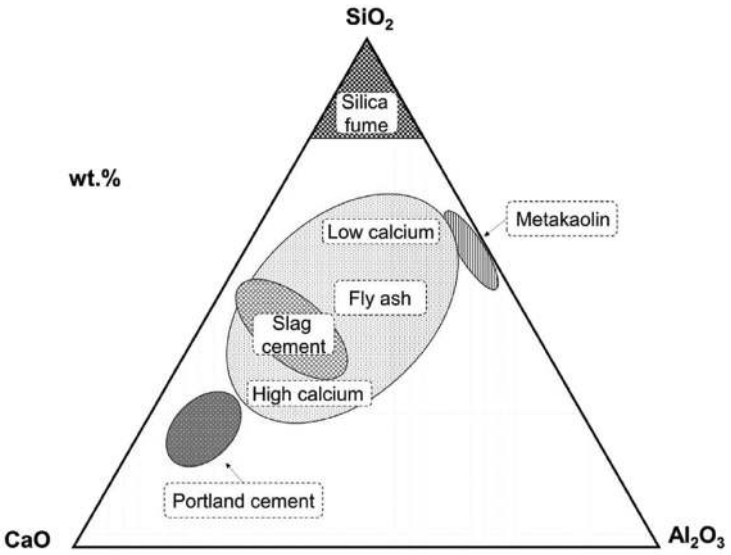

FIGURE 2.3 – Ternary diagram of the most common precursors (GIERGICZNY, 2019).

2.3.1.1 Low-calcium systems

The most common materials are industrial by-products like Class F fly ash (FA) or thermally activated natural resources such as calcined clays, like metakaolin (MK). The predominant products are N-A-S-H gels, which structure is amorphous, highly cross-linked, and chemically resembles a disordered zeolite, offering superior thermal stability, chemical resistance, and reduced shrinkage, though typically requiring longer curing time and temperature between 80-100 °C to reach the appropriate mechanical strength (PROVIS *et al.*, 2014; PROVIS; BERNAL, 2014; KE *et al.*, 2021; NODEHI; TAGHVAEE, 2022).

2.3.1.2 High-calcium systems

High-calcium AAMs are derived from precursors rich in CaO, making them chemically closer to traditional hydraulic cements. The main precursors are materials such as ground granulated blast furnace slag (GGBFS). The primary reaction product is an aluminum-substituted calcium silicate hydrate (C-A-S-H) gel, which is structurally similar to the C-S-H found in Portland cement but incorporates aluminum in its structure. The C-A-S-H gel formed in alkali-activated GGBFS typically has a lower Ca/Si ratio than hydrated Portland cement (PROVIS *et al.*, 2014; SEGURA *et al.*, 2023). These systems exhibit rapid strength development and good early-age performance but are more susceptible to shrinkage, cracking, and corrosion due to chloride attack.

2.3.1.3 Hybrid systems

Mixtures containing both calcium and aluminosilicate-rich materials, such as blast furnace slag (BFS) combined with FA or MK, or systems containing low levels of Portland cement, where both C-A-S-H and N-A-S-H phases coexist, potentially optimizing mechanical strength and durability (PACHECO-TORGAL *et al.*, 2014; LUUKKNEN Z. ABDOLLAHNEJAD, 2017; PROVIS *et al.*, 2014).

2.3.2 Activators

The alkaline attack on the microstructure of the precursors results in the release of silicates and aluminates into the solution. Hence, the solubility of silica and alumina is important for studies in this field, which can be expressed as a function of pH (Figure 2.4).

It is observed that the solubility of silica is low in acidic environments and high in basic media, while alumina is soluble at both extremes of pH. Therefore, for the activation reactions to occur, it is necessary that the pH of the solution is high. The main alkaline activators are: sodium hydroxide (NaOH), sodium silicate (Na_2SiO_3), potassium hydroxide (KOH), sodium carbonate (Na_2CO_3) and potassium carbonate (K_2CO_3).

Alkaline activators can form two different systems: (i) one-part systems are designed as dry powder mixtures incorporating the precursor and a solid alkaline activator, requiring only the addition of water ("just-add-water"), this approach enables factory production, bagging, and distribution analogous to conventional cement (PROVIS, 2018); and (ii) two-part systems, where liquid alkaline solutions are prepared separately and then mixed with the precursor

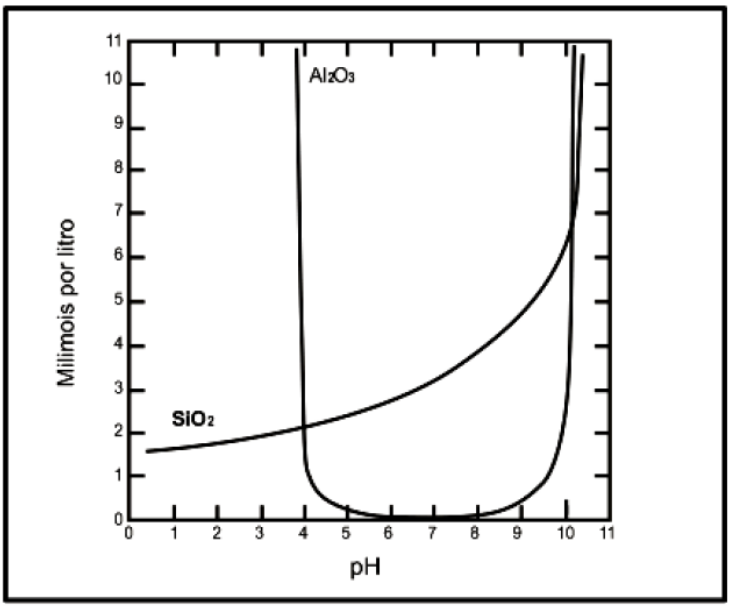

FIGURE 2.4 – Solubility of silica and alumina as a function of pH (MASON, 1952).

2.4 Current Limitations and Research Gaps

Despite the numerous advantages of alkali-activated materials, several challenges hinder their widespread adoption in the construction industry.

2.4.1 Safety Concerns

The first studies on AAMs focused on two-part systems, since the final product exhibits high compressive strength, adhesion, and the ability to withstand fatigue loads. In addition, they also demonstrate high resistance to freeze-thaw cycles and high temperatures (HEATH *et al.*, 2014).

However, two-part systems require the mixing of a solid precursor with a concentrated aqueous alkaline solution at the point of use. These solutions are corrosive and irritate human skin, making their transport and handling hazardous for workers (AWOYERA, 2019).

The need to handle highly corrosive, viscous, and often hazardous activator solutions in the field is a major impediment to their practicality, mixing, and large-scale market adoption (SHAH *et al.*, 2020).

2.4.2 Alternative sources

The availability and long-term supply of conventional industrial by-products remain a challenge. GGBFS and FA are the most popular precursors, with GGBFS often yielding the highest mechanical strength (QIN *et al.*, 2022). However, the supply of FA is projected to decrease globally due to the shift away from coal energy, and BFS availability depends on local availability from the iron-making industry (PACHECO-TORGAL *et al.*, 2014). This necessitates extensive research focused on optimizing mixes using precursors other than fly ash and blast furnace slag. For systems targeting low-calcium AAMs, this means exploring less conventional, locally available low-Ca aluminosilicate solid waste resources (RAKHIMOVA, 2022).

2.4.3 Environmental impacts

The main environmental advantage attributed to AAMs lies in the considerable reduction of CO_2 emissions compared to traditional Portland cement. It is estimated that the environmental impacts of solid and liquid activators are 24% and 60% of the impact caused by OPC, respectively (LUUKKNEN Z. ABDOLLAHNEJAD, 2017).

However, the production of sodium silicate - which is the main alkaline activator used in one-part AAM with low-calcium precursors (LUUKKNEN Z. ABDOLLAHNEJAD, 2017) - occurs between 1200-1400°C and emits approximately 1.514 kg of CO_2 per kg of silicate produced, in addition to significantly contributing to air pollution through dust and nitrogen and sulfur oxides (RAJAN, 2020). Indeed, some studies show that the emissions profile of certain alkali-activated concrete/binders (AACB) mixtures can be worse than OPC if synthetic activators dominate the material composition (PACHECO-TORGAL *et al.*, 2014).

Therefore, a crucial research gap lies in the pursuit of alternative and environmentally friendly solid alkaline sources that are sodium silicate free or require minimal synthetic input (LUUKKNEN Z. ABDOLLAHNEJAD, 2017).

2.5 Justification of the present research

This research directly addresses the limitations in three ways: (i) practicality; (ii) precursor diversity; and (iii) environmental impact.

By developing a one-part mix system, this study eliminates the need for handling corrosive liquid alkaline activators, promoting user-friendly product commercialization and simplifying logistics for construction applications.

By utilizing low-calcium solid precursors (instead of high-calcium), the research contributes to diversifying the raw materials base and reducing reliance on traditional industrial by-products whose availability is increasingly strained or declining.

By concentrating on non-hazardous and less polluting solid alkaline sources, this work aims to develop an environmentally and economically competitive binder, contributing significantly to the reduction of the construction industry's carbon and ecological footprint.

In essence, this work provides necessary scientific investigation into optimizing the mix design for the next generation of alkali-activated binders: cost-effective, easily deployable (one-part), and truly sustainable systems based on low-calcium precursors and eco-friendly activation agents.

3 Methodology

3.1 Materials

For the development of one-part alkali activated pastes and mortars, the following components were used:

- Kaolin supplied by the company Brasilminas;
- Silica fume (SF) supplied by the company Elken;
- Potassium carbonate supplied by the company Neon (purity of 98%);
- Calcium hydroxide supplied by the company Neon (purity of 95%);
- Standardized quartz sand supplied by the company Instituto de Pesquisas Tecnológicas (IPT);
- Distilled water.

The precursors used were silica fume and metakaolin - which was produced from commercial kaolin, as detailed in Section 3.2.1.1. The alkaline sources are commercially available with high purity, so the physicochemical compositions provided by the manufacturer were used.

In addition, the quartz sand used follows the standards established by the Institute for Technological Research (IPT), as shown in Tables 3.1 and 3.2.

TABLE 3.1 – Results of physical and chemical requirements of standardized quartz sand, following ABNT NBR7214:2015 requirements.

Property	Result	Requirement	Reference
Silica content	96.5%	$\geq$ 95%, by mass	NBR14656:2001
Moisture	0.0%	$\leq$ 0.2%, by mass	NBR7214:2015
Organic matter	Lighter or equal to the color of the standard solution	Color of the 2% tannic acid standard solution	NBR17053:2022

TABLE 3.2 – Particle size distribution of the fractions of standardized quartz sand, following ABNT NBR7214:2015 requirements.

Fraction	Sieve interval	Mass percentage (%)	
		Result	Requirement
16	(2.4 mm and 2.0 mm)	0	≤ 10
16	(2.0 mm and 1.2 mm)	97	≥ 90
30	(1.2 mm and 0.6 mm)	99	≥ 95
50	(0.6 mm and 0.3 mm)	96	≥ 95
100	(0.3 mm and 0.15 mm)	95	≥ 95

3.2 Methods

The experimental process was divided into three steps: (i) production and characterization of raw-materials; (ii) production of geopolymeric pastes and mortars; (iii) microstructural studies and physical properties of hardened state.

3.2.1 Production and Characterization of Raw Materials

3.2.1.1 Production of Metakaolin

Metakaolin was obtained by calcining kaolin at 700 °C for 1 hour in a 200 L 18 kW laboratory furnace. The optimal calcination time and temperature were determined from preliminary tests, in which the yield of calcination and reactivity was evaluated. To ensure material homogeneity, two shallow trays with a maximum height of 10 mm were used. The transformation of crystalline kaolinite into amorphous metakaolinite is represented by Equation 3.1.

$$Al_2.Si_2O_5\,(OH)_4 \xrightarrow{\Delta} Al_2O_3.2SiO_2 + 2H_2O \tag{3.1}$$

3.2.1.2 Physicochemical Characterization of Solid Precursors

The physicochemical characterization of the solid precursors was carried out at the laboratories of the Aeronautics Institute of Technology (ITA), located in São José dos Campos-SP.

The oxide compositions of metakaolin and silica fume were determined by X-ray Fluorescence (XRF). To complement this XRF analysis, the removal of hydroxyl groups (OH^-) was verified by loss on ignition (LOI). The results were used to calculate the Si/Al molar ratios and to verify the purity of the precursors.

In addition, X-ray diffraction (XRD) was used to verify the absence crystalline phases

of metakaolin and silica fume, as they are amorphous. XRD was performed by a Panalytical Empyrean diffractometer, with a 2θ interval of 10-70°, Cu-Kα radiation, 0.01° step and 50 s/step.

To verify the presence of bonds, Fourier-transform infrared spectroscopy (FTIR) was carried out in a PerkinElmer spectrophotometer, with a spectrum range of 4000-400 cm^{-1} and a spectral resolution of 1 cm^{-1}.

3.2.2 Production of Geopolymeric Pastes and Mortars

3.2.2.1 Mix Design

The development of one-part geopolymeric mortars followed a systematic experimental design, aiming to evaluate the effect of different compositions on physicochemical and mechanical properties.

The variable of interest in this experiment is the Si/Al ratio, which will be varied from 0.9 to 5.0, calculated based on the proportion of metakaolin and silica fume.

The following proportions were considered constant in this study:

- Mass ratio water/solids (w/s);
- Molar ratio Al/K;
- Molar ratio K/Ca;
- Mass ratio sand/binder for mortars (s/b).

Initially, the water-to-solids ratio was determined to ensure adequate workability of the pastes, targeting a spread diameter of 200-250 mm in the mini-slump test.

In addition, due to stoichiometric balance, the Al/K ratio will be constant and equal to 1, according to the empirical formula on Equation 3.2 (DAVIDOVITS, 1991), where M is a sodium or potassium cation.

$$M_n \left\{ \left(SiO_2\right)_z AlO_2 \right\}_n \cdot wH_2O \tag{3.2}$$

Furthermore, the K/Ca ratio will be constant and equal to 2, respecting the precipitation reaction of potassium carbonate with calcium hydroxide, as shown in Equation 3.3.

$$K_2CO_3 + Ca(OH)_2 \rightarrow 2KOH_{(aq)} + CaCO_{3(s)} \downarrow \tag{3.3}$$

With the paste proportions well defined, the production of mortars maintained a 1:2 ratio between binder and sand, analogously in the previous researches (BATISTA *et al.*, 2025) and (ARELLANO-AGUILAR *et al.*, 2014).

3.2.2.2 Mixing Procedure

The production of the mixtures followed standardized procedures. For the production of mortars and compressive strength testing, the procedures of the European standard (EUROPEAN COMMITTEE FOR STANDARDIZATION (CEN), 2016) were followed. For the production of pastes, the American standard (ASTM, 2006) was chosen, since the Brazilian standard does not specify the mixing procedure for cementitious pastes without fine aggregate. Both procedures were adapted for the preparation of small-volume samples.

3.2.2.3 Molding and Curing of Specimens

For the compressive strength test and bulk density/water absorption measurements, the specimens were prepared in prismatic molds with dimensions $40 \times 40 \times 40\ mm$, previously lubricated with oil-based release agent.

For each composition, 9 specimens were molded, 3 were intended for testing at ages of 1 day, and 6 at 3 days. It was not necessary to perform tests at longer curing ages, as the thermal curing of the binders used provides high initial strength gain (AREDES *et al.*, 2015).

Thermal curing was carried out in an oven maintained at (60 ± 2) °C and a minimum relative humidity of 95% for 24 hours, as recommended by the standard (ABNT, 2006), to ensure the activation of the binders and accelerate the curing process. By curing at this temperature it is possible to minimize the pore volume, therefore achieve higher compressive strength (AREDES *et al.*, 2015). It is noteworthy that demolding was performed 24 hours after the start of the curing process. After demolding, the specimens were immediately transferred to the corresponding curing conditions until the testing age.

These samples were stored in hermetically sealed containers to prevent rehydration.

3.2.3 Microstructural studies and physical properties of hardened state

3.2.3.1 Characterization of Geopolymeric pastes

The microstructural characterization of the hardened pastes was performed by X-ray diffraction (XRD), Fourier-transform infrared spectroscopy (FTIR), Helium-pycnometer density, mercury intrusion porosimetry (MIP) and scanning electron microscopy (SEM)

with energy-dispersive X-ray spectroscopy (EDS).

Moreover, XRD and FTIR were performed under the same conditions applied for the raw materials. However, since both techniques require fine powders, small samples were grinded, then, the polymerization was interrupted by immersion in ethyl alcohol - as it is a dehydrating agent that does not react with the components of the geopolymeric paste- and vacuum filtration, followed by drying in an oven at 50°C for 24 hours.

Finally, Energy-dispersive X-ray spectroscopy (EDS) was performed together with scanning electron microscopy (SEM) to evaluate the morphology of the hardened pastes. SEM/EDS was conducted using a TESCAN VEGA 3 XMU device and Oxford EDS 133 eV detector, with gold coated.

3.2.3.2 Helium Pycnometer Density

The true density was determined by gas pycnometry. A gas pycnometer measures the true volume of a solid-even if porous-by monitoring the gas pressure variation in a chamber of known volume. Helium is commonly used because it is inert and readily penetrates accessible pores, allowing for a more accurate determination of the solid volume.

The helium pycnometer consists of two chambers of known volumes (previously calibrated): the sample chamber and the expansion chamber, connected by an expansion valve. Before the analysis, the sample placed in the sample chamber undergoes degassing by repeated helium purges to remove impurities and moisture. After bringing the system to atmospheric pressure, the expansion chamber is isolated (closing the expansion valve), and the sample chamber is pressurized to P_1 (about 17 psi). Then the expansion valve is opened, leading to a pressure drop to P_2. Assuming ideal behavior of helium, the solid volume can be obtained from:

$$P_1 \, (V_a - x) \;=\; P_2 \, (V_a - x + V_e), \tag{3.4}$$

or equivalently,

$$V_s \;=\; V_a \;-\; \frac{V_e}{\dfrac{P_1}{P_2} - 1}, \tag{3.5}$$

where V_a is the sample-chamber volume, V_e is the expansion-chamber volume, x is the solid volume, and V_s denotes the same solid volume as the final expression.

The bulk density is automatically calculated by the instrument from the ratio between the solid mass (previously obtained on a balance and provided as input) and the volume derived from the equation above.

The main advantage of this method is its ability to measure only the volume of the solid

substance, discounting all open (gas-accessible) pores. In principle, it can also measure solids at any moisture content. A limitation is the maximum specimen size, constrained by the sample holder capacity (up to 10 cm^3).

3.2.3.3 Mercury Intrusion Porosimetry

This technique is based on the principle that the mercury intrusion under controlled pressure is a function of the pore diameters, according to Laplace's equation:

$$d = -\frac{4\,\gamma\cos\theta}{P}, \tag{3.6}$$

where γ is the interfacial tension between mercury and air (0.48 $N\,m^{-1}$), P is the applied pressure (2-5000 psi), θ is the contact angle (130°), and d is the pore diameter.

The total porosity was determined from:

$$P = \frac{V_{\mathrm{MP}}}{V_{\mathrm{MP}} + \dfrac{M_a}{\rho}}, \tag{3.7}$$

where P is the total porosity, V_{MP} is the volume of mercury intruded, M_a is the sample mass, and ρ is the sample density.

The test was performed on an AMINCO (American Instrument Company) Model 5-7118 instrument.

3.2.3.4 Physical properties of mortars

Water absorption and apparent density tests were conducted on the hardened mortars to evaluate their porosity-related properties. These tests followed the procedures established by the ASTM C642-13 standard (ASTM International, 2013) which provides guidelines for determining the volume of permeable voids through oven-drying, immersion, and weighting steps.

Additionally, for the compressive strength test, the specimens were placed in a hydraulic press with a 600 kN-load limit, applying load at a rate of 0.5 kN/s until failure. The strength was calculated by the equation:

$$R_c = \frac{F_c}{A_t} \tag{3.8}$$

where R_c is the compressive strength (in MPa), F_c is the maximum applied load (in N), and A_t is the cross-sectional area (in mm^2).

For statistical analysis, the Tukey test was performed, allowing the identification of significant differences between sample groups, considering a significance level of 95%. The Table 3.3 summary presents the summary of the methods used in this work.

TABLE 3.3 – Summary of tests performed, samples used, curing conditions and main objetives.

Test	Precursors	Si/Al ratios	Curing days	Objetive
XRF	Yes	–	–	Determination of oxide content to calculate molar ratios
LOI	Yes	–	–	Assessment of hydroxyl removal and quantification of volatile matter
XRD	Yes	0.9 - 5.0	3	Identification of crystalline and amorphous phases
FTIR	Yes	0.9 - 5.0	1, 3	Identification of chemical bonds in order to monitor the geopolymerization
He pycnometry/MIP	No	0.9, 3.0, 5.0	3	Determination of pore size distribution and total porosity
SEM/EDS	No	0.9, 3.0, 5.0	3	Observation of morphology and elemental distribution
Water absorption and apparent density	No	0.9 - 5.0	3	Measurement water absorption and bulk density
Compressive strength	No	0.9 - 5.0	1, 3	Evaluation of mechanical performance

4 Results and Discussion

4.1 Chemical and Physical Characterization of Precursors

4.1.1 Chemical Composition of Precursors

The chemical composition of the aluminosilicate precursors plays a fundamental role in determining their reactivity and suitability for activation in a low-calcium system. In this work, the metakaolin (MK) and silica fume (SF) precursors were analysed with XRF for their oxide content (normalized with respect to the powder fraction) and loss on ignition (LOI), which was found to be 0.69% and 2.27%, respectively.

TABLE 4.1 – Chemical composition (wt %) of the precursors: metakaolin (MK) and silica fume (SF).

Oxide	Metakaolin wt (%)	Silica Fume wt (%)
K_2O	0.21	0.74
CaO	0.19	0.13
MgO	2.60	0.00
Cl	0.00	0.12
SO_3	0.00	0.15
SiO_2	49.37	96.90
Fe_2O_3	0.77	1.78
Al_2O_3	46.38	0.00
Na_2O	0.00	0.17
TiO_2	0.49	0.00

From Table 4.1.1 it is clear that the MK precursor is rich in alumina and contains a significant silica fraction , while the SF is extremely high in silica and essentially alumina-free. Critically, both materials present very low CaO contents. The minimal presence of calcium oxide is an important indicator of the low-calcium nature of the precursors, which is a pre-requisite for favoring the formation of potassium aluminosilicate hydrate type gels, rather than calcium-rich gels, as often observed when using ground granulated blast furnace slag (ALI *et al.*, 2023).

In addition, the low LOI values suggest a limited amount of residual organics or

volatile components, which could otherwise interfere with the dissolution kinetics of the aluminosilicates. Furthermore, the Si/Al molar ratio of MK precursors is approximately 0.9, which will be used with the essentially pure SF to tailor the mix designs for optimal geopolymerization reactions.

The formulations are based on varying Si/Al ratios while maintaining constant Al/K ratio of 1.0, K/Ca ratio of 2.0 and water/solids ratio of 0.45 for all formulations. For the mortar samples, a constant sand-to-binder ratio of 2.0 was maintained to ensure comparable workability and mechanical properties across all mix designs.

TABLE 4.2 – Mix design formulations for paste samples with varying Si/Al ratios.

Sample	Alkaline Source	Si/Al	Mass (g)			
			MK	SiO_2	$K_2CO_3/Ca(OH)_2$	Water
5.0	$K_2CO_3/Ca(OH)_2$	5.0	8.68	20.39	8.59	16.95
4.0	$K_2CO_3/Ca(OH)_2$	4.0	10.02	17.78	9.91	16.97
3.0	$K_2CO_3/Ca(OH)_2$	3.0	11.84	14.23	11.71	17.01
2.0	$K_2CO_3/Ca(OH)_2$	2.0	14.48	9.10	14.32	17.05
0.9	$K_2CO_3/Ca(OH)_2$	0.9	19.15	0.00	18.95	17.14

TABLE 4.3 – Mix design formulations for mortar samples with varying Si/Al ratios.

Sample	Source	Si/Al	Mass (g)					
			MK	SiO_2	K_2CO_3	$Ca(OH)_2$	Water	Sand
5.0	$K_2CO_3/Ca(OH)_2$	5.0	88.93	208.82	56.65	31.33	173.58	771.47
4.0	$K_2CO_3/Ca(OH)_2$	4.0	102.55	182.03	65.33	36.13	173.72	772.07
3.0	$K_2CO_3/Ca(OH)_2$	3.0	121.10	145.54	77.15	42.66	173.90	772.90
2.0	$K_2CO_3/Ca(OH)_2$	2.0	147.84	92.94	94.18	52.09	174.17	774.09
0.9	$K_2CO_3/Ca(OH)_2$	0.9	195.09	0.00	124.28	68.73	174.64	776.20

In summary, the chemical data confirm that both MK and SF meet the key requirements of (i) high silica and/or alumina content, (ii) low calcium content, and (iii) minimal impurities, thereby validating their use as raw materials for a low calcium alkali-activated binder system.

4.1.2 X-Ray Diffraction of Precursors and Alkaline Sources

XRD analysis of the alkaline sources revealed distinct crystalline characteristics. The XRD patterns of SF and MK displayed broad amorphous humps, characteristic of disordered aluminosilicate and silica networks (PROVIS; DEVENTER, 2009; KE *et al.*, 2021). In MK, a diffuse hump centered around $2\theta \approx 21°$ was observed, with minor peaks corresponding to residual quartz (COD 900-9667), indicating the presence of impurities,

which remains inert during calcination (PROVIS; BERNAL, 2014) and acts as filler without participating in geopolymerization reaction (RAKHIMOVA; RAKHIMOV, 2019a). The SF diffractogram showed a similar amorphous feature near $2\theta \approx 22.5°$, confirming the predominance of a non-crystalline silica phase with no detectable crystalline impurities.

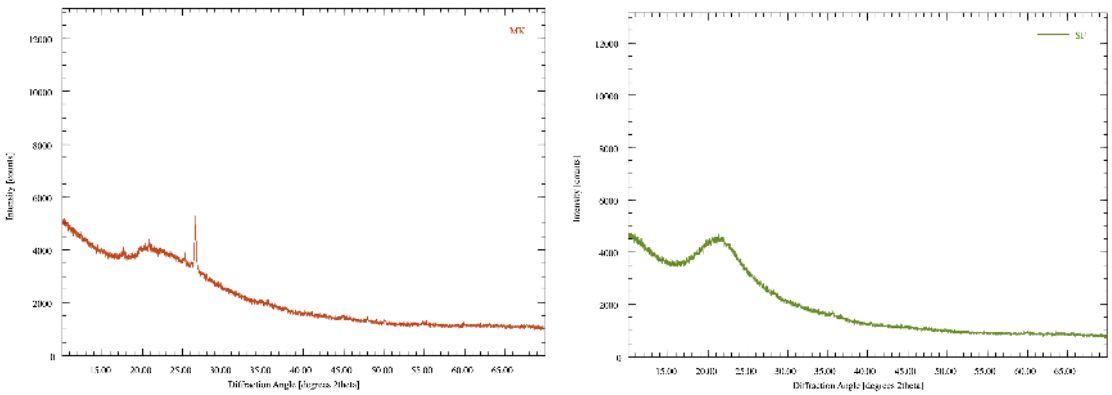

(a) Metakaolin (MK) (b) Silica Fume (SF)

FIGURE 4.1 – XRD patterns of solid precursors.

These findings align with the literature, where metakaolin typically exhibits a predominantly amorphous structure with residual quartz peaks depending on the calcination temperature and source clay, while silica fume is almost entirely amorphous as it is a by-product of the smelting process in silicon and ferrosilicon alloy production (PACHECO-TORGAL *et al.*, 2014). The high amorphous content of these precursors is advantageous for geopolymerization, as it enhances the dissolution of reactive aluminosilicate species and promotes the formation of N-A-S-H and K-A-S-H type gels, leading to improved mechanical performance (QIN *et al.*, 2022).

The diffractogram of K_2CO_3 exhibited reflections attributed to crystalline potassium carbonate (COD 900-9644). Similarly, the spectrum of $Ca(OH)_2$ showed well-defined peaks corresponding to the portlandite phase (COD 900-0114), confirming its high crystallinity and purity.

These results are consistent with findings from previous studies that identified portlandite and alkali carbonates as highly crystalline solids used in geopolymer and alkali-activated systems due to their strong reactivity and predictable phase behavior (PROVIS; DEVENTER, 2014).

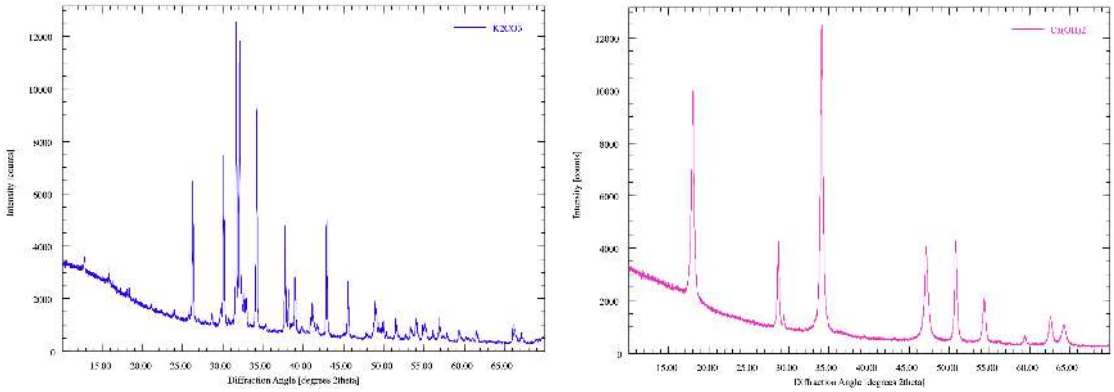

(a) Potassium Carbonate (K_2CO_3) (b) Calcium Hydroxide ($Ca(OH)_2$)

FIGURE 4.2 – XRD patterns of alkaline sources.

4.1.3 Fourier Transform Infrared Spectroscopy of Precursors

For the aluminosilicate precursors, the metakaolin exhibited three main bands at 623, 787, and 1051 cm^{-1}, while the silica fume showed two bands at 799 and 1040 cm^{-1}. For MK, the intense band at 1051 cm^{-1} corresponds to the asymmetric stretching vibration of the Si-O-T bonds (where T is Si or Al) and is characteristic of its disordered aluminosilicate network, while lower wavenumber bands, such as 623 cm^{-1} and 787 cm^{-1}, relate to bending vibrations like Si-O-Al and Al-O-T (MORAES *et al.*, 2024).

Conversely, the SF spectrum shows its main band at 1040cm^{-1}, also attributed to Si-O-T stretching, but the SF is highly pure, lacking significant Al content (as seen by the XRF results in Table 4.1), meaning this peak is dominated by Si-O-Si bonds. The second, smaller band near 799 cm^{-1} is related to the symmetric stretching of the Si-O-Si network, likely residual quartz or the amorphous silica structure (MA *et al.*, 2022).

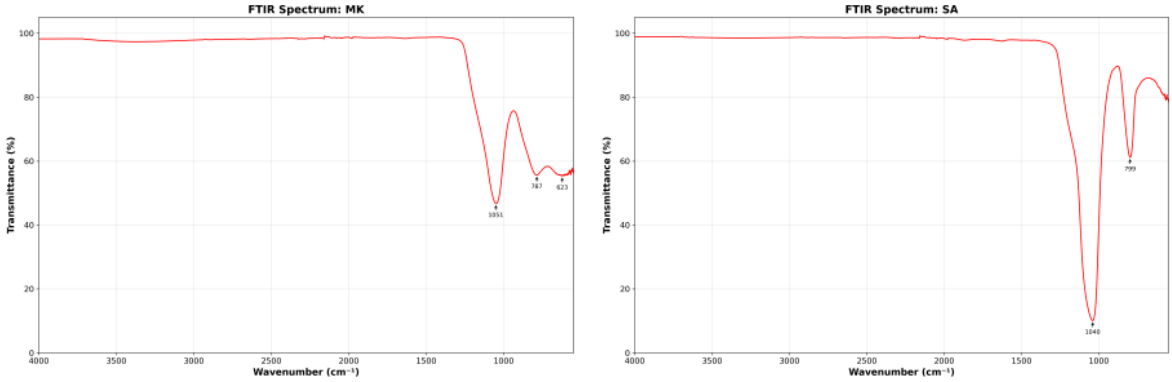

(a) Metakaolin (MK) (b) Silica Fume (SF)

FIGURE 4.3 – FTIR spectra of solid precursors.

The spectral signatures of MK and SF validate their suitability as precursors for low-calcium alkali-activated system. MK serves as the primary source of both reactive Al_2O_3

and SiO_2. Silica Fume, characterized by its amorphous nature and high SiO_2 content, is included primarily to adjust the overall Si/Al ratio of the system. Both precursors possess the amorphous structure required, and their dominant high-frequency Si-O-T peaks confirm the presence of the structural units necessary to form the cross-linked K-A-S-H gel phase in the final binder (PROVIS *et al.*, 2014).

Turning to the alkaline sources, the K_2CO_3 exhibited peaks at 706, 879, 1061, 1360, and 3177 cm^{-1}. The bands at 879 cm^{-1} and 1360 cm^{-1} reinforce the existence of C-O bonds (MORAES *et al.*, 2024). The broader peak at 3177 cm^{-1} is often attributed to O-H stretching (BRITO *et al.*, 2008), likely from adsorbed water or moisture inherent to the hygroscopic nature of the alkaline salt.

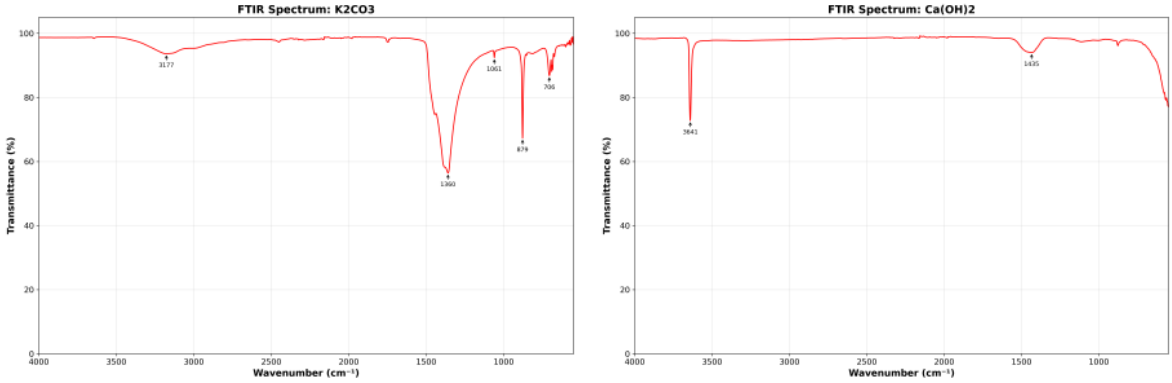

(a) Potassium Carbonate (K_2CO_3) (b) Calcium Hydroxide ($Ca(OH)_2$)

FIGURE 4.4 – FTIR spectra of alkaline sources.

Similarly, $Ca(OH)_2$ presented two primary peaks at 1435 cm^{-1} and 3641 cm^{-1}. The sharp peak at 3641 cm^{-1} is attributed to the stretching vibration of the O-H groups in portlandite, a feature noted in several studies on alkaline activated materials (BATISTA *et al.*, 2025). The secondary, broader band observed near 1435 cm^{-1} is associated with the asymmetric stretching vibration of carbonate (O-C-O) bonds, specifically indicating the presence of carbonates impurities (ZHAO *et al.*, 2023).

These results align well with existing literature concerning alkaline precursors. The carbonate peaks observed in both $Ca(OH)_2$ and K_2CO_3 powders strongly suggest partial carbonation, a common occurrence either during handling, storage, or the sample preparation process (LEI *et al.*, 2021).

4.2 Microstructural Characterization of Pastes

4.2.1 X-Ray Diffraction

X-ray diffraction patterns after 3-day curing of the pastes at different Si/Al ratios (Figure 4.5) showed a persistent amorphous hump in all compositions, indicating the presence of aluminosilicate gel (K-A-S-H). It is also is important to note that the intensity of peaks are stronger for lower Si/Al ratios, which is related to the higher content of crystalline phases, mainly calcite, which is easier to be detected by XRD due to its high crystallinity.

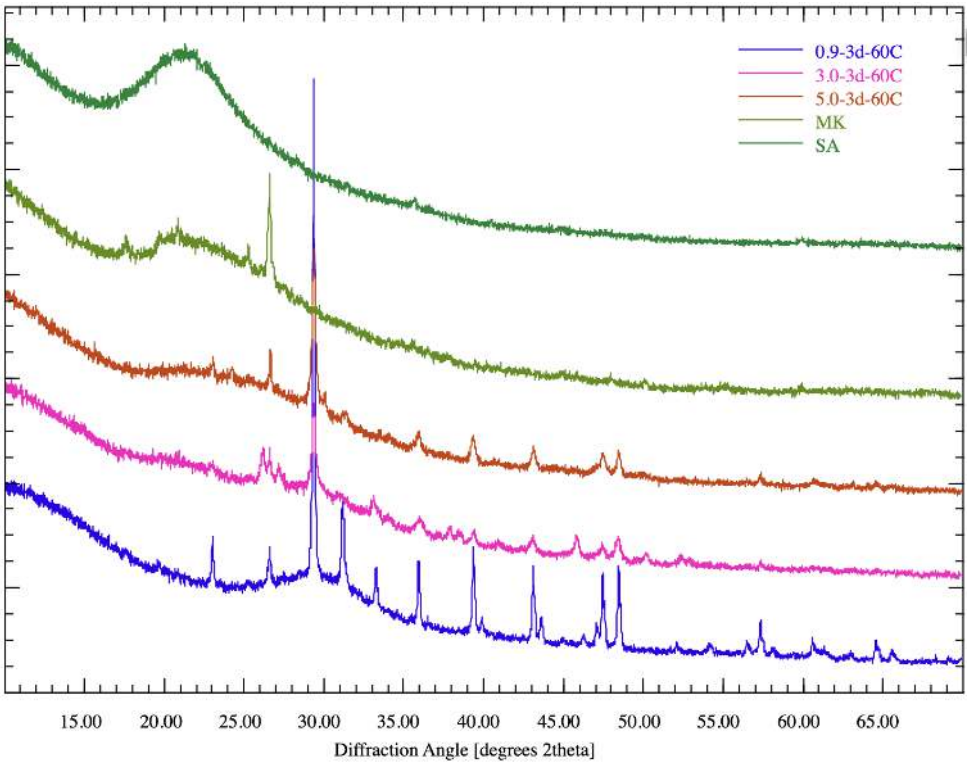

FIGURE 4.5 – XRD patterns of pastes at different Si/Al ratios after 3 days of curing.

In agreement with other studies, the geopolymerization process-which is responsible for the strength-is indicated by the presence of the broad hump among $2\theta = 20 \approx 35°$ - shifted the location of the amorphous hump to lower angles as the silica proportion increases (ARELLANO-AGUILAR *et al.*, 2014; LEE *et al.*, 2017; WAN *et al.*, 2017).

The patterns of the pastes show sharp peaks of crystalline phases of solid precursors, this indicates that the they were not involved in the geopolymerization process (GERALDO, 2020), but were rather present as inactive fillers, as noted by (RUIZ-SANTAQUITERIA *et al.*, 2012). Additionally, there was no peaks from portlandite observed in any of the pastes, confirming its complete reaction. The crystalline phases identified in the XRD patterns are presented in Table 4.4, showing the semi-quantitative phase composition at 3 days for

different Si/Al ratios.

TABLE 4.4 – Semi-quantitative crystalline phases at 3 days for different Si/Al ratios (XRD).

Phase (%)	Si/Al				
	0.9	2.0	3.0	4.0	5.0
Calcite ($CaCO_3$)	77	56	43	52	79
Butschliite ($K_2Ca(CO_3)_2$)	18	29	0	0	0
Aragonite ($CaCO_3$)	0	0	41	24	0
Quartz (SiO_2)	6	14	16	17	21
Stishovite (SiO_2)	0	0	0	7	0

4.2.2 Fourier Transform Infrared Spectroscopy

FTIR spectra were collected for all pastes after 1 and 3 days of curing to analyze the chemical bonding and structural changes associated with geopolymerization at different Si/Al ratios. There was no significant variation in the spectra from 1 to 3 days of curing, so only the spectra after 3 days are represented in Figure 4.6.

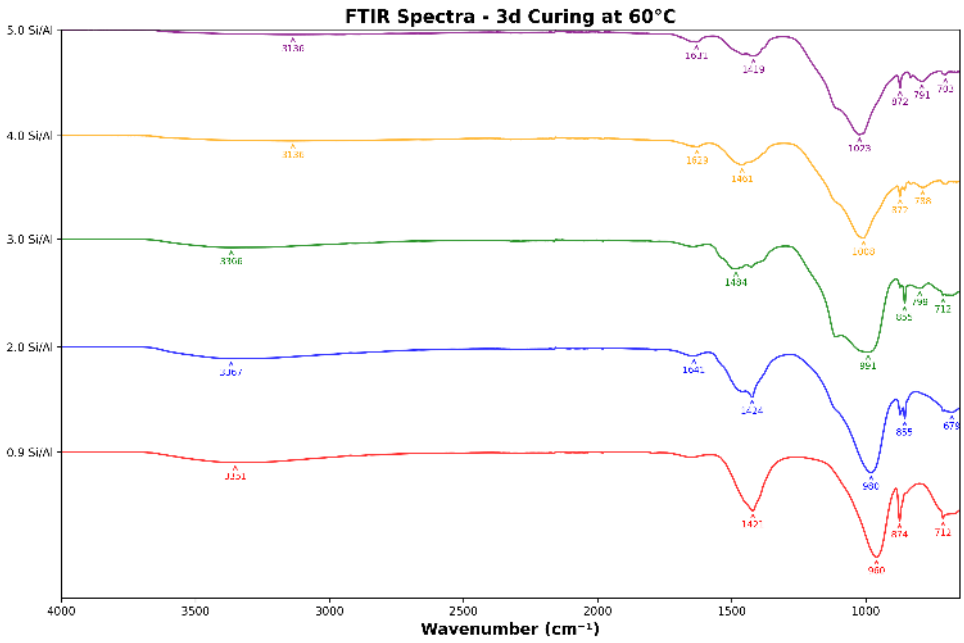

FIGURE 4.6 – FTIR spectra of pastes at different Si/Al ratios after 3 days of curing.

The key to interpreting these spectra lies in the fingerprint region (400-1200 cm^{-1}), which reflects the formation of the polymeric network, and the hydroxyl/carbonate regions (1300-3700 cm^{-1}), which indicate water and carbonation.

At lower Si/Al ratios, the reaction leads to a network with a higher density of Si-O-Al bonds, while the increasing Si content promotes the formation of Si-O-Si linkages, resulting in a more siliceous gel structure. Consequently, the main band of Figure 4.6

shifts from approximately 960 cm^{-1} (Si/Al = 0.9) to 1023 cm^{-1} (Si/Al = 5.0). This shift toward higher wavenumbers indicates a higher degree of polymerization and a stronger molecular network, since the replacement of AlO_4^- by SiO_4^- tetrahedra increases the bond energy of the Si-O-T (T = Si or Al) structure (PACHECO-TORGAL *et al.*, 2014; MA *et al.*, 2022; PROVIS; DEVENTER, 2009).

The carbonate-related bands near 1400 cm^{-1} (1419-1484 cm^{-1}) were detected in all compositions, corresponding to C-O stretching in carbonates. However, as the Si/Al ratio increased, these peaks became broader and less defined. This behavior suggests that different types of carbonates coexist in the matrix - mainly $CaCO_3$ and K_2CO_3 - as confirmed by XRD analysis (Figure 4.4). The coexistence of multiple carbonate species, each with slightly different crystallographic structures, contributes to the overlapping and broadening of the absorption band.

A "shoulder" around 1100 cm^{-1} becomes more evident with increasing Si content. This feature is generally attributed to asymmetric Si-O-Si stretching vibrations in silicate-rich frameworks (MA *et al.*, 2022). Its absence in the Si/Al = 0.9 paste and progressive definition at higher Si contents indicate the increasing contribution of unreacted or reprecipitated silica phases. This band confirms the presence of silicate polymerization products and supports the observation that Si-enriched mixtures lead to the formation of a more Si-O-Si-dominated network.

The complete disappearance of the 3641 cm^{-1} band, characteristic of crystalline portlandite (Figure 4.4), indicates that all $Ca(OH)_2$ initially added reacted completely within 3 days of curing, aligned with the XRD results. This confirms the high reactivity of $Ca(OH)_2$ under thermal curing at 60 °C and its full participation in the reaction with K_2CO_3 to generate the alkaline environment required for activation.

Finally, the peak around 790 cm^{-1}, present only in pastes with Si/Al greater than 3.0, corresponds to unreacted silica. Its absence in samples with Si/Al = 0.9 and 2.0 suggests a more complete dissolution and reaction of the silica fume at intermediate Si/Al ratios. Therefore, considering both the 790 cm^{-1} silica band and the overall gel polymerization trends, the optimal composition appears to be between Si/Al = 2.0 and 3.0, where the degree of reaction and structural homogeneity are maximized.

4.2.3 Porosity

Helium gas pycnometry results (Table 4.5) showed that the paste with Si/Al = 3.0 exhibited the highest density among the analyzed compositions, followed by Si/Al = 0.9 and Si/Al = 5.0. This behavior correlates well with the mercury intrusion porosimetry data presented in Table 4.6, which revealed that the Si/Al = 3.0 paste also possesses the

lowest total porosity and a more refined pore network compared to the other mixtures. The increase in density is therefore consistent with the development of a denser aluminosilicate matrix, suggesting a more advanced geopolymerization reaction and improved packing efficiency of the reaction products at this intermediate Si/Al ratio.

TABLE 4.5 – Density results of the samples by He-pycnometry .

Sample	Density (g/cm^3)	Average Density (g/cm^3)	Standard Deviation
0.9-3d-60°C	2.1663	2.170	0.002
	2.1715		
	2.1686		
	2.1716		
	2.1712		
3.0-3d-60°C	2.1846	2.184	0.002
	2.1866		
	2.1806		
	2.1820		
	2.1843		
5.0-3d-60°C	2.1547	2.139	0.009
	2.1350		
	2.1388		
	2.1345		
	2.1342		

In contrast, the paste with Si/Al = 0.9 presented a comparable porosity level to that of the Si/Al = 3.0 composition, but with a larger average pore diameter, indicating a less compact microstructure. The mixture with Si/Al = 5.0, on the other hand, displayed a coarser pore size distribution and lower apparent density, which can be attributed to its reduced workability and the highly viscous, cohesive behavior of the fresh paste, leading to inefficient particle dispersion and air entrapment during casting. Similar rheological limitations at elevated Si/Al ratios have been reported by (GERALDO, 2020), who associated the increase in mixture viscosity with an incomplete dissolution of the silicate precursor.

TABLE 4.6 – Results obtained from mercury intrusion porosimetry tests.

Sample	Porosity (%)	80% of pores (μm)	Average diameter (μm)	Penetration (cm^3/g)
0.9-3d-60°C	42.51	Between 0.7 and 0.25	0.625	0.34
3.0-3d-60°C	42.82	Between 0.16 and 0.0051	0.12	0.34
5.0-3d-60°C	46.71	Between 1.75 and 0.065	0.097	0.40

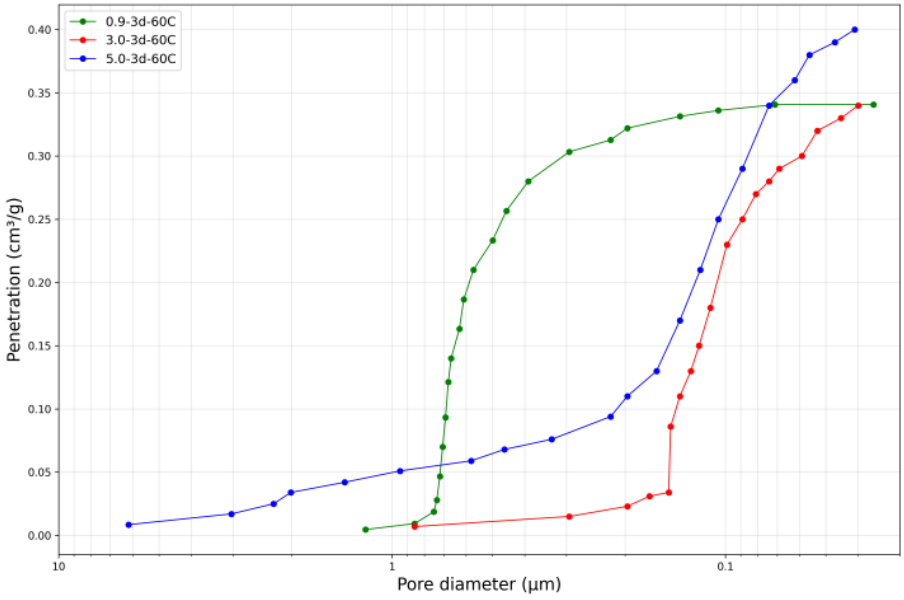

FIGURE 4.7 – Mercury intrusion curves as a function of pore diameter for the samples.

4.2.4 Scanning Electron Microscopy and Energy Dispersive Spectroscopy

Scanning electron microscopy analyses of the pastes cured for 3 days revealed a clear dependence of matrix morphology on the Si/Al molar ratio.

At a Si/Al ratio of 0.9, the EDS images showed a high frequency of unreacted precursor particles, particularly calcite (green regions in Figure 4.9), which was also identified in the XRD patterns (Table 4.5). These particles are likely formed when free alkalis are not completely incorporated into the aluminosilicate gel and subsequently react with atmospheric CO_2 to precipitate as carbonates (PROVIS, 2018). The microstructure displayed numerous pores (dark voids) of similar diameter to those measured by mercury intrusion porosimetry (Table 4.6), confirming consistency between both techniques. Furthermore, the EDS map (blue points in Figure 4.9) indicated a high occurrence of unreacted metakaolin particles, suggesting that low Si/Al compositions result in incomplete dissolution and heterogeneous gel formation. The layered EDS image (Figure 4.9a) also evidenced surface heterogeneity in this paste.

In contrast, the paste with Si/Al = 3.0 exhibited the densest and most homogeneous matrix among all compositions, with fewer unreacted particles and a continuous gel phase. This morphology indicates that intermediate Si/Al ratios favor an optimal balance between the dissolution of aluminosilicates and the condensation of the K-A-S-H gel, resulting in a compact structure. This is visually supported by the continuous orange regions observed in the EDS layered image (Figure 4.11a). The smaller pore sizes relative to Si/Al = 0.9 corroborate the porosimetry results (Table 4.6). Carbonate crystals, identified as aragonite and calcite (green regions in Figure 4.11b), were detected but in lower frequency, indicating reduced carbonation compared to the low-silica system.

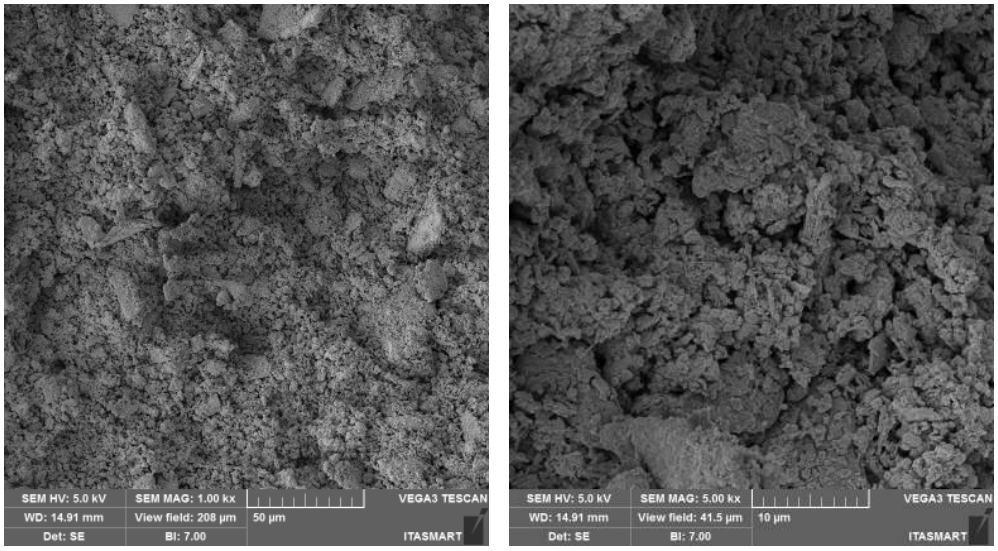

(a) 1000× magnification (b) 5000× magnification

FIGURE 4.8 – SEM micrographs of paste with Si/Al = 0.9 after 3 days of curing (spot 5).

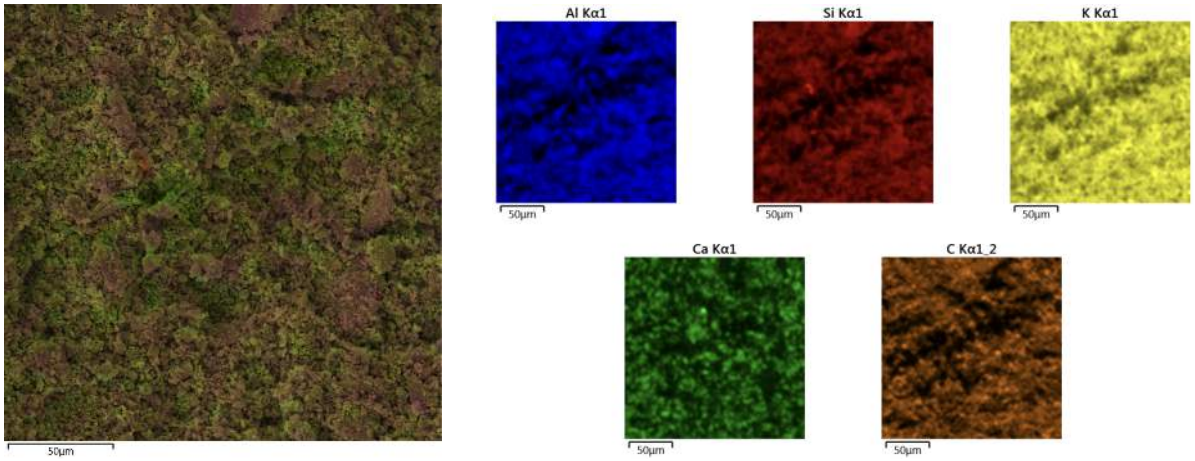

(a) EDS layered image (b) EDS map

FIGURE 4.9 – EDS analysis of Spot 5, Si/Al = 0.9, cured for 3 days at 60°C at 1000× magnification.

At a Si/Al ratio of 5.0, the microstructure became less compact and presented numerous unreacted silicate particles, suggesting that excessive silica content exceeds the dissolution and polymerization capacity of the system. These particles appear as purple regions in the EDS maps (Figure 4.13) and are consistent with the strong Si-O-Si vibration observed near 1100 cm^{-1} in the FTIR spectra (Figure 4.6). The pore structure was notably coarser than that of the Si/Al = 3.0 paste, consistent with the MIP results (Table 4.6). Unreacted silica fume particles (red regions in Figure 4.13b) were also visible, confirming incomplete dissolution. Additionally, distinct calcium carbonate crystals (green regions) were identified, possibly formed within casting voids later filled by carbonation, as indicated by the XRD data (Table 4.4).

Futhermore, the K/Al ratio was also found to be higher than expected, which may

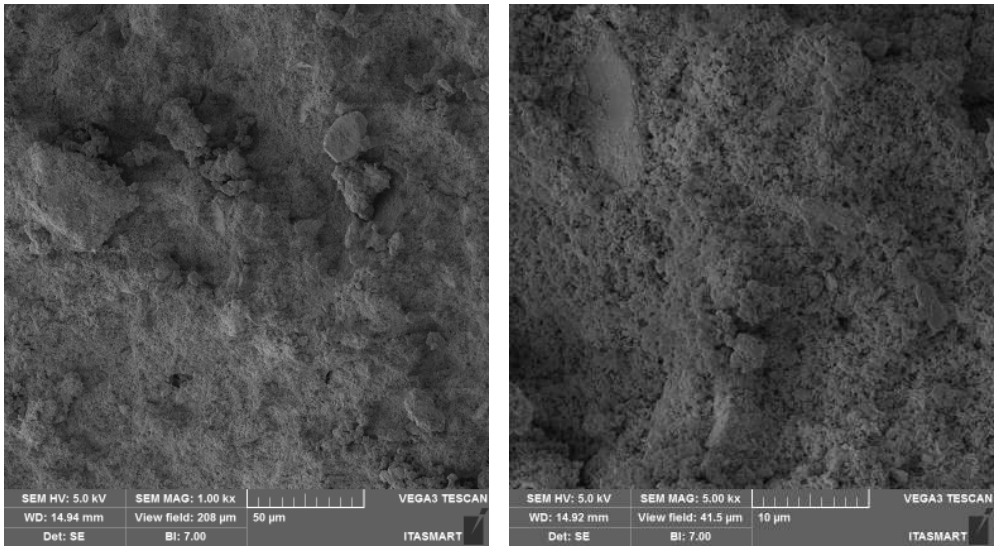

(a) 1000× magnification (b) 5000× magnification

FIGURE 4.10 – SEM micrographs of paste with Si/Al = 3.0 after 3 days of curing (spot 3).

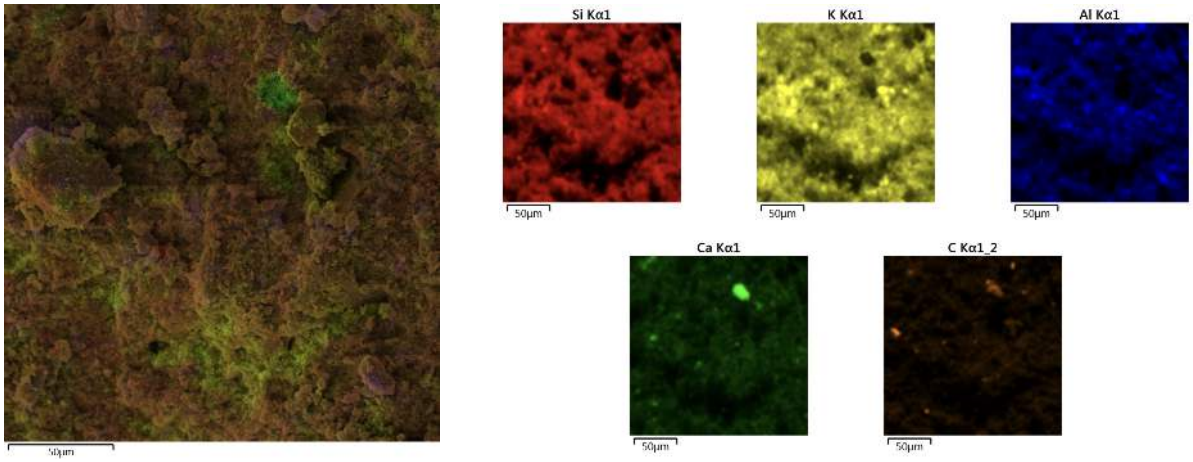

(a) EDS layered image (b) EDS map

FIGURE 4.11 – EDS analysis of Spot 3, Si/Al = 3.0, cured for 3 days at 60°C at 1000× magnification.

indicate a preferential incorporation of atmospheric CO_2, leading to the formation of potassium carbonate on the surface. It is also important to note that EDS is a surface technique and the analyzed spots may not be precise for quantitative analysis, since it was not performed on polished sections neither with large areas.

The quantitative EDS results are summarized in Table 4.7. The K/Ca ratio remained approximately constant (≈2), consistent with the stoichiometric proportion defined in the mix design. However, the Si/Al ratios obtained were slightly higher than the intended nominal values, possibly due to the higher solubility of silica in the alkaline medium and its slower incorporation into the gel network (CHEN *et al.*, 2024). The Al/K ratio was also marginally lower, which may indicate the superficial formation of potassium carbonate through atmospheric carbonation. It is worth noting that EDS provides localized

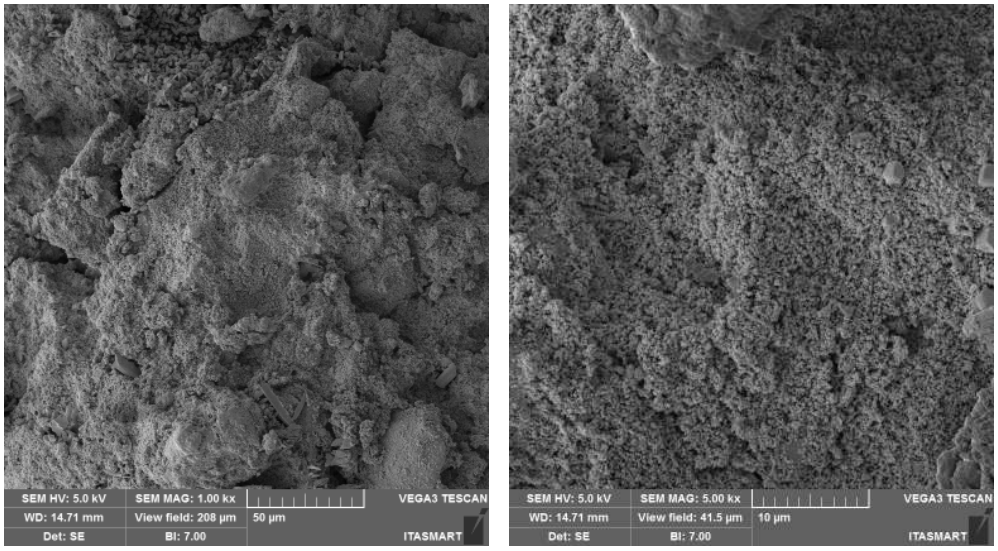

(a) 1000× magnification (b) 5000× magnification

FIGURE 4.12 – SEM micrographs of paste with Si/Al = 5.0 after 3 days of curing (spot 1).

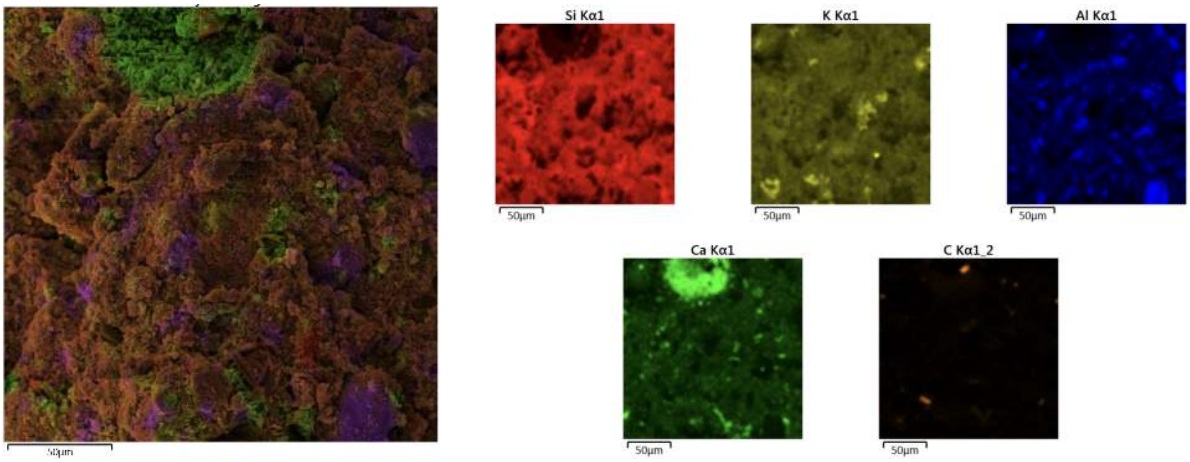

(a) EDS layered image (b) EDS map

FIGURE 4.13 – EDS analysis of Spot 1, Si/Al = 5.0, cured for 3 days at 60°C at 1000× magnification.

surface analysis; hence, the results should be interpreted preferably qualitatively, as the measurements were not taken on polished or large-area sections.

TABLE 4.7 – EDS spectrum of pastes after 3 days of curing at 60°C.

Sample	At(%)				Atomic ratio		
	Si	Al	K	Ca	Si/Al	Al/K	K/Ca
0.9_60C_3d_Spot5	26.4	27.1	30.4	16.0	0.97	0.89	1.90
3.0_60C_3d_Spot3	54.2	13.5	21.5	10.8	4.01	0.63	2.00
5.0_60C_3d_Spot1	59.5	9.2	19.6	11.6	6.47	0.47	1.69

Additional EDS spectral data for all analyzed spots can be found in Appendix A.

4.3 Physical properties of Mortars

4.3.1 Bulk density and water absorption

The bulk density results for the mortars are presented in Table 4.8. Among the compositions studied, the mixture with a Si/Al ratio of 3.0 exhibited the highest bulk density (2.425 ± 0.009 g/cm^3). This finding is consistent with the He-pycnometry results for the corresponding pastes (Table 4.5), which also indicated a denser matrix for this composition. The correlation between these two analyses suggests that at this intermediate Si/Al ratio the geopolymerization reaction was more advanced, resulting in greater packing efficiency of the reaction products and reduced microstructural voids, as also supported by the MIP data (Table 4.6).

TABLE 4.8 – Bulk density, water absorption, and permeable voids volume of mortars (curing for 3 days at 60°C).

Sample	Absorption (%)	Bulk density (g/cm^3)	Permeable voids volume (%)
0.9_3d-60C	11.0 ± 0.1	2.407 ± 0.008	21.5 ± 0.2
2.0_3d-60C	11.6 ± 0.1	2.401 ± 0.014	22.3 ± 0.7
3.0_3d-60C	11.9 ± 0.1	2.425 ± 0.009	23.1 ± 0.3
4.0_3d-60C	11.5 ± 0.2	2.404 ± 0.011	22.4 ± 0.2
5.0_3d-60C	11.3 ± 0.3	2.399 ± 0.008	21.5 ± 0.4

Despite presenting the highest bulk density, the Si/Al = 3.0 mortar showed the highest water absorption (11.9 ± 0.1 %) and permeable void volume (23.1 ± 0.3 %). This result appears counterintuitive when compared with mercury-intrusion porosimetry, since conventional cementitious systems usually exhibit an inverse relationship between density and porosity. However, water absorption depends not only on total porosity but also on the affinity between water and the solid matrix. In alkali-activated materials, water molecules interact strongly with the aluminosilicate network, enabling penetration by capillary action even through nanoscale pores. Conversely, mercury is a non-wetting, inert fluid that requires external pressure to enter pores; it does not interact chemically with the surface and is less sensitive to narrow or tortuous pore geometries. As discussed in previous studies (PROVIS *et al.*, 2014), this discrepancy between techniques arises because MIP may underestimate connectivity in complex pore networks due to the "ink-bottle" effect.

During the immersion stage of the absorption test, a visible color difference was observed in the storage water between samples of different Si/Al ratios, suggesting partial dissolution or leaching of soluble components. This phenomenon is consistent with the release of residual alkali species from the matrix into solution, as reported by previous studies on alkali-activated systems (PACHECO-TORGAL *et al.*, 2014). Such behavior indicates that the K-A-S-H gel network may contain weakly bound alkalis or unreacted

phases that are susceptible to ion exchange processes. Similar findings in the literature have shown that prolonged water exposure can destabilize aluminosilicate frameworks when excess alkalis are present, leading to gradual degradation of the geopolymer matrix (BRITO *et al.*, 2008).

Overall, the joint interpretation of bulk density, absorption, and porosity results confirms that the Si/Al = 3.0 composition yields the most compact and refined matrix.

4.3.2 Compressive strength

Table 4.9 reports the compressive strength of the mortars at 1 day and 3 days of curing at 60 ° C for Si/Al ratios of 0.9, 2.0, 3.0, 4.0, and 5.0, while Figure 4.14 summarizes the trend across ages.

TABLE 4.9 – Compressive strength of mortars cured at 60°C after 1 and 3 days.

Si/Al ratio	Compressive Strength (MPa)	
	1 day	3 days
0.9	5.91 ± 0.08	7.83 ± 0.40
2.0	14.56 ± 0.64	14.44 ± 0.49
3.0	22.16 ± 0.82	23.88 ± 0.35
4.0	14.83 ± 0.25	16.85 ± 1.95
5.0	12.91 ± 0.21	14.68 ± 0.08

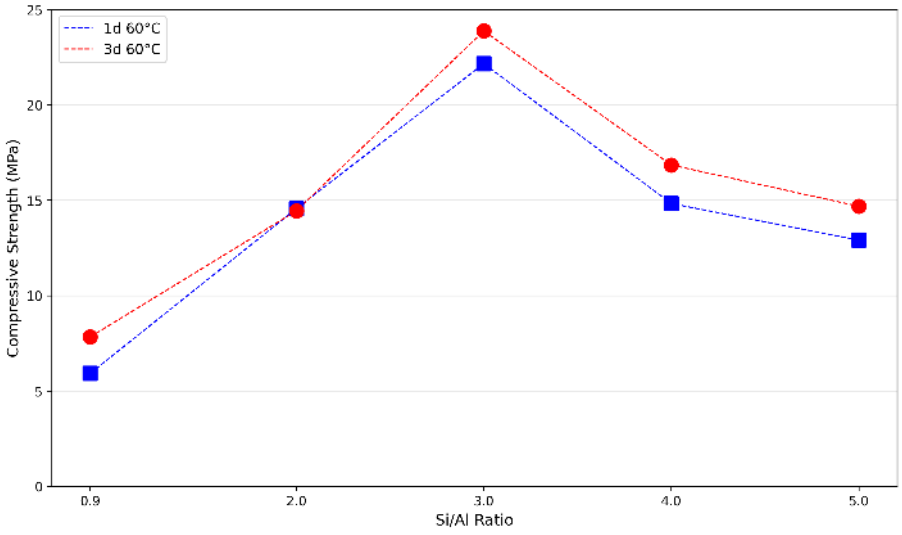

FIGURE 4.14 – Comparison of compressive strength for mortars cured for 1 day and 3 days at 60°C.

A one-way ANOVA performed separately for each curing age indicated a significant effect of composition on strength. Tukey's HSD post hoc tests confirmed that Si/Al=3.0 had significantly higher strength than all other mixtures, while Si/Al=0.9 had significantly lower strength than all others. At 1 day, Si/Al=2.0 and 4.0 were statistically indistin-

guishable, whereas at 3 days, Si/Al=2.0, 4.0, and 5.0 did not differ significantly from one another.

Between 1 day and 3 days, the strength increased consistently for all mix designs, consistent with continued gel polymerization and densification under thermal curing. This aligns with the disappearance of the portlandite band and the evolution of a more cross-linked aluminosilicate network.

The superior performance of Si/Al=3.0 is consistent with a more advanced and efficient geopolymer network. FTIR spectra showed a shift of the main Si-O-T band from approximately 960 cm^{-1} at low Si/Al to 1023 cm^{-1} at higher Si/Al, indicating increased polymerization and stronger bond energy in the aluminosilicate framework as SiO_4 progressively substitutes AlO_4. XRD results revealed a dominant amorphous hump and absence of crystalline portlandite, while low Si/Al mixtures exhibited more intense carbonate peaks—evidence of unreacted solids that have no significant contribution to strength.

Density data also support these findings: Si/Al=3.0 achieved the highest paste and mortar densities, indicating a more compact matrix. Mercury intrusion porosimetry showed that total porosity of Si/Al=3.0 was similar to that of 0.9, yet its pore system was markedly refined, with 80% of pores between 0.16 and 0.005μm (versus 0.70-0.25μm for 0.9). This refinement limits stress concentrators and enhances load-bearing capability. SEM-EDS observations confirmed a compact and homogeneous gel at Si/Al=3.0, with fewer unreacted particles and less carbonate crystallization compared to 0.9 or 5.0.

Although Si/Al=5.0 had higher total porosity (46.7%) than 0.9 (42.5%), its much finer average pore diameter ($\sim$0.097μm vs. $\sim$0.625μm) reduced stress concentrations and improved strength performance, leading to the conclusion that, for this system, pore refinement was more critical to strength than total porosity.

The existence of an optimal Si/Al ratio around 3 is consistent with prior studies. Arellano-Aguilar (ARELLANO-AGUILAR *et al.*, 2014) reported similar behavior for low-grade metakaolin-based mortars. Lee (LEE *et al.*, 2017) found that the amorphous Si/Al ratio of fly ash strongly governs strength development, with a maximum near Si/Al=3.5 (for similar curing conditions of this work). Wan (WAN *et al.*, 2017) confirmed through simulation and microstructural analysis that beyond this ratio, unreacted silica increases and strength decreases.

5 Conclusion

This study successfully developed a one-part alkali-activated system composed of low-calcium solid precursors (MK and SF) and alternative alkaline sources (K_2CO_3 and $Ca(OH)_2$). The results demonstrated that the proposed formulation is technically viable, producing stable and compact matrices with adequate mechanical performance and improved safety and sustainability compared to conventional alkali-activated systems.

The variation of the Si/Al molar ratio directly influenced both the polymerization kinetics and the microstructural characteristics of the binders. Mixtures with Si/Al=3.0 achieved the best balance between density, porosity, and mechanical strength, reflecting an optimal degree of geopolymerization and a more homogeneous gel formation. Samples with low Si/Al ratios showed the presence of unreacted particles and larger pore sizes, whereas high Si/Al formulations tended to exhibit excessive viscosity, hindering workability and leading to heterogeneous matrices.

The microstructural analyses (XRD, FTIR and SEM/EDS) confirmed the formation of predominantly amorphous aluminosilicate gels (K-A-S-H), where the gel characteristics and composition depended on the precursor proportion. MIP and He pycnometry observed different pore distribution and matrix structures. This results reflected in the compressive strength tests, which indicated a significant increase over time due to the continuous condensation of silicate and aluminate species.

Overall, the study demonstrates that combining MK and SF with mild alkaline sources is a promising strategy for developing safer and more environmentally benign binders. The use of K_2CO_3 and $Ca(OH)_2$ effectively activated the aluminosilicate network, achieving mechanical and microstructural properties comparable to those of more hazardous systems based on NaOH or sodium silicate.

Future work should expand the range of solid precursors to include natural, locally available aluminosilicate materials similar to MK and SF, like volcanic tuffs or agricultural ashes. Exploring their synergy with alternative activators under varied curing conditions will yield insights for performance optimization and large-scale applicability. Additionally, long-term durability studies under diverse environmental exposures are recommended to confirm the practical potential of these one-part AAM for construction use.

Bibliography

ABNT. **ABNT NBR 9479:2006 - Argamassa e concreto — Câmaras úmidas e tanques para cura de corpos-de-prova**. 2. ed. Rio de Janeiro, Brasil, maio 2006. Válida a partir de 30 de junho de 2006.

ALI, S. A.; TAHIR, M. F.; REHMAN, S.; SIDDIQUE, R.; RANA, M. A.; FAROOQ, M.; KHAN, W. A. Geopolymer chemistry and composition: A comprehensive review of synthesis, reaction mechanisms, and material properties—oriented with sustainable construction. **Case Studies in Construction Materials**, Elsevier, v. 19, p. e02089, 2023.

ANDREW, R. M. Global co2 emissions from cement production. **Earth System Science Data**, Copernicus GmbH, v. 10, n. 1, p. 195–217, 2018.

AREDES, F.; CAMPOS, T.; MACHADO, J.; SAKANE, K.; THIM, G.; BRUNELLI, D. Effect of cure temperature on the formation of metakaolinite-based geopolymer. **Ceramics International**, Elsevier, v. 41, n. 6, p. 7302–7311, 2015.

ARELLANO-AGUILAR, R.; BURCIAGA-DÍAZ, O.; GOROKHOVSKY, A.; ESCALANTE-GARCÍA, J. I. Geopolymer mortars based on a low grade metakaolin: Effects of the chemical composition, temperature and aggregate: binder ratio. **Construction and Building Materials**, Elsevier, v. 50, p. 642–648, 2014.

ASTM. **ASTM C305: Standard Practice for Mechanical Mixing of Hydraulic Cement Pastes and Mortars of Plastic Consistency**. West Conshohocken, PA, USA, 2006. Designação oficial: ASTM C305-06.

ASTM International. **ASTM C642-13: Standard Test Method for Density, Absorption, and Voids in Hardened Concrete**. West Conshohocken, PA, USA, 2013. Designation: C642-13.

AWOYERA, A. A. P. O. A critical review on application of alkali activated slag as a sustainable composite binder. **Miscellaneous**, v. 11, p. e00268–e00268, 2019.

BATISTA, J.; CORDEIRO, G.; RIBEIRO, L.; MORAES, J. Improved microstructure and compressive strength of pastes and mortars containing mgo-sio2 cement produced by combined calcination of mgco3 and kaolin. **Cement and Concrete Composites**, v. 157, p. 105959, 2025.

BERNAL, S. A.; GUTIÉRREZ, R. M. de; PROVIS, J. L. Engineering and durability properties of alkali-activated slag concretes. **Construction and Building Materials**, Elsevier, v. 33, p. 99–108, 2014.

BRASIL. **Política Nacional de Resíduos Sólidos: Lei nº 12.305, de 2 de agosto de 2010, e legislação correlata**. 3. ed. Brasília, 2016. (Série Legislação, n. 230). Atualizada até 12 de fevereiro de 2016.

BRITO, M.; CASE, E.; KRIVEN, W. M. (Ed.). **Developments in Porous, Biological and Geopolymer Ceramics**. Hoboken, NJ: Wiley-Interscience / American Ceramic Society, 2008. (Ceramic Engineering and Science Proceedings, v. 28). ISBN 9780470196403.

CHEN, Y.; LIMA, L. M. de; LI, Z.; MA, B.; LOTHENBACH, B.; YIN, S.; YU, Q.; YE, G. Synthesis, solubility and thermodynamic properties of nash gels with various target si/al ratios. **Cement and Concrete Research**, Elsevier, v. 180, p. 107484, 2024.

DAVIDOVITS, J. Geopolymers: Inorganic polymeric new materials. **Journal of Thermal Analysis and Calorimetry**, v. 37, p. 1633–1656, 08 1991.

DUXSON A. FERNÁNDEZ-JIMÉNEZ, J. L. P. P. Geopolymer technology: the current state of the art. **EBSCOhost Academic Search Premier**, v. 42, n. 9, p. 2917–2933, 2006.

EUROPEAN COMMITTEE FOR STANDARDIZATION (CEN). **EN 196-1:2016 - Methods of Testing Cement - Part 1: Determination of Strength**. Brussels, Belgium, 2016. Supersedes EN 196-1:2005+A1:2008. Available at: https://standards.cen.eu/.

GERALDO, R. H. **Aglomerante álcali-ativado de parte única: obtenção, composição, propriedades e durabilidade**. Thesis (Tese de Doutorado) — Universidade Estadual de Campinas, Campinas, Brasil, 2020. Orientadora: Profa. Dra. Gladis Camarini.

GIERGICZNY, Z. Fly ash and slag. **Cement and Concrete Research**, v. 124, p. 105826, 2019. ISSN 0008-8846.

HEATH, A.; PAINE, K.; MCMANUS, M. Minimising the global warming potential of clay based geopolymers. **Journal of Cleaner Production**, v. 78, p. 75–83, 2014.

KE, X.; BERNAL, S. A.; PROVIS, J. L. One-part alkali-activated materials: State-of-the-art and perspectives. **Cement and Concrete Research**, Elsevier, v. 140, p. 106336, 2021.

LEE, B.; KIM, G.; KIM, R.; CHO, B.; LEE, S.; CHON, C.-M. Strength development properties of geopolymer paste and mortar with respect to amorphous si/al ratio of fly ash. **Construction and Building Materials**, Elsevier, v. 151, p. 512–519, 2017.

LEI, J.; LAW, W. W.; YANG, E.-H. Effect of calcium hydroxide on the alkali-silica reaction of alkali-activated slag mortars activated by sodium hydroxide. **Construction and Building Materials**, v. 272, p. 121868, 2021.

LUUKKNEN Z. ABDOLLAHNEJAD, J. Y. T. One-part alkali-activated materials: A review. **Elsevier ScienceDirect Journals**, v. 103, p. 21–34, 2017.

MA, B.; LUO, Y.; ZHOU, L.; SHAO, Z.; LIANG, R.; FU, J.; WANG, J.; ZANG, J.; HU, Y.; WANG, L. The influence of calcium hydroxide on the performance of mk-based geopolymer. **Construction and Building Materials**, v. 329, p. 127224, 2022.

MASON, B. Principles of geochemistry. **Miscellaneous**, v. 74, n. 3, p. 262, 1952.

MORAES, J.; MORAES, M.; BATISTA, J.; AKASAKI, J.; FONT, A.; TASHIMA, M.; SORIANO, L.; BORRACHERO, M.; PAYÁ, J. Influence of sugar cane straw ash in metakaolin-based geopolymers. **Construction and Building Materials**, v. 444, p. 137835, 2024.

NEUPANE, K. Evaluation of environmental sustainability of one-part geopolymer binder concrete. **Cleaner Materials**, Elsevier, v. 6, p. 100138, 2022.

NODEHI, M.; TAGHVAEE, V. M. Alkali-activated materials and geopolymer: a review of common precursors and activators addressing circular economy. **Circular Economy and Sustainability**, v. 2, p. 165–196, 2022.

PACHECO-TORGAL, F.; LABRINCHA, J.; LEONELLI, C.; PALOMO, A.; CHINDAPRASIRT, P. (Ed.). **Handbook of Alkali-Activated Cements, Mortars and Concretes**. Oxford, UK: Elsevier, 2014. ISBN 9781782422884.

PROVIS, J. L. Alkali-activated materials. **Nature Reviews Materials**, Nature Publishing Group, v. 3, n. 6, p. 276–277, 2018.

PROVIS, J. L.; BERNAL, S. A. Geopolymers and related alkali-activated materials. **Annual Review of Materials Research**, Annual Reviews, v. 44, p. 299–327, 2014.

PROVIS, J. L.; DEVENTER, J. S. J. van (Ed.). **Geopolymers: Structure, Processing, Properties and Industrial Applications**. Cambridge, UK: Woodhead Publishing / CRC Press, 2009. ISBN 9781845694494.

PROVIS, J. L.; DEVENTER, J. S. J. van (Ed.). **Alkali Activated Materials: State-of-the-Art Report, RILEM TC 224-AAM**. [*S.l.*]: Springer, 2014. (RILEM State-of-the-Art Reports, v. 13). ISBN 978-94-007-7671-5.

PROVIS, J. L.; FERNÁNDEZ-JIMÉNEZ, A.; KAMSEU, E.; LEONELLI, C.; PALOMO, A. Binder chemistry - low-calcium alkali-activated materials. *In*: PROVIS, J. L.; DEVENTER, J. S. J. van (Ed.). **Alkali Activated Materials: State-of-the-Art Report, RILEM TC 224-AAM**. [*S.l.*]: Springer, 2014. p. 93–124.

QIN, Y.; QU, C.; MA, C.; ZHOU, L. One-part alkali-activated materials: State of the art and perspectives. **Polymers**, v. 14, n. 22, p. 5046, 2022.

QUÉRÉ, C. L.; ANDREW, R. M.; FRIEDLINGSTEIN, P.; SITCH, S.; PONGRATZ, J.; MANNING, A. C.; KORSBAKKEN, J. I.; PETERS, G. P.; CANADELL, J. G.; JACKSON, R. B. *et al.* Global carbon budget 2017. **Earth System Science Data**, Copernicus GmbH, v. 10, n. 1, p. 405–448, 2018.

RAJAN, P. K. H. S. Sustainable development of geopolymer binder using sodium silicate synthesized from agricultural waste. **Elsevier ScienceDirect Journals**, v. 286, p. 124959–124959, 2020.

RAKHIMOVA, N. R. Recent advances in blended alkali-activated cements: a review. **European Journal of Environmental and Civil Engineering**, v. 26, n. 10, p. 4596–4618, 2022.

RAKHIMOVA, N. R.; RAKHIMOV, R. Z. Reaction products, structure and properties of alkali-activated metakaolin cements incorporated with supplementary materials - a review. **Journal of Materials Research and Technology**, v. 8, n. 1, p. 1522–1531, 2019.

RAKHIMOVA, N. R.; RAKHIMOV, R. Z. Reaction products, structure and properties of alkali-activated metakaolin cements incorporated with supplementary materials–a review. **Journal of Materials Research and Technology**, Elsevier, v. 8, n. 1, p. 1522–1531, 2019.

RUIZ-SANTAQUITERIA, C.; SKIBSTED, J.; FERNÁNDEZ-JIMÉNEZ, A.; PALOMO, A. Alkaline solution/binder ratio as a determining factor in the alkaline activation of aluminosilicates. **Cement and Concrete Research**, Elsevier, v. 42, n. 9, p. 1242–1251, 2012.

SCRIVENER, K. L.; JOHN, V. M.; GARTNER, E. M. Eco-efficient cements: Potential economically viable solutions for a low-co2 cement-based materials industry. **Cement and concrete Research**, Elsevier, v. 114, p. 2–26, 2018.

SEGURA, I. P.; RANJBAR, N.; DAMø, A. J.; JENSEN, L. S.; CANUT, M.; JENSEN, P. A. A review: Alkali-activated cement and concrete production technologies available in the industry. **Heliyon**, v. 9, p. e15718, 2023.

SEVERO, C. G. S.; COSTA, D. L.; BEZERRA, I. M. T.; MENEZES, R. R.; NEVES, G. A. Características, particularidades e princípios científicos dos materiais ativados alcalinamente. **Revista Eletrônica de Materiais e Processos**, v. 8, n. 2, p. 55–67, 2013.

SHAH, S. F. A.; CHEN, B.; ODERJI, S. Y.; HAQUE, M. A.; AHMAD, M. R. Comparative study on the effect of fiber type and content on the performance of one-part alkali-activated mortar. **Construction and Building Materials**, v. 243, p. 118221, 2020.

KELLY, T. D.; MATOS, G. R. (Ed.). **Cement Statistics - Historical Statistics for Mineral and Material Commodities in the United States**. Reston, VA, USA, 2016. (U.S. Geological Survey Data Series, 140).

VINAI, R.; SOUTSOS, M. Production of sodium silicate powder from waste glass cullet for alkali activation of alternative binders. **Cement and Concrete Research**, Elsevier, v. 116, p. 45–56, 2019.

WAN, Q.; RAO, F.; SONG, S.; GARCÍA, R. E.; ESTRELLA, R. M.; PATIÑO, C. L.; ZHANG, Y. Geopolymerization reaction, microstructure and simulation of metakaolin-based geopolymers at extended si/al ratios. **Cement and Concrete Composites**, Elsevier, v. 79, p. 45–52, 2017.

ZAREECHIAN, M.; SIAD, H.; LACHEMI, M.; SAHMARAN, M. Advancements in cleaner production of one-part geopolymers: A comprehensive review of mechanical properties, durability, and microstructure. **Elsevier ScienceDirect Journals**, v. 409, p. 133876–133876, 2023.

ZHAO, Q.; MA, C.; HUANG, B.; LU, X. Development of alkali activated cementitious material from sewage sludge ash: Two-part and one-part geopolymer. **Journal of Cleaner Production**, v. 384, p. 135547, 2023.

Appendix A - EDS Spectra

This appendix presents the complete collection of EDS images for all analyzed spots across different Si/Al ratios. All specimens were cured for 3 days at 60°C and 1000× magnification. For each Si/Al ratio, atomic and weight percentages spectra are provided for each analyzed spot.

A.1 Si/Al = 0.9

TABLE A.1 – EDS spectrum of Si/Al = 0.9 pastes after 3 days of curing at 60°C.

Sample	At(%)				Wt(%)			
	Si	Al	K	Ca	Si	Al	K	Ca
0.9_60C_3d_Spot1	22.9	26.6	34.1	16.4	19.1	21.4	39.9	19.6
0.9_60C_3d_Spot2	26.5	28.9	31.1	13.7	22.7	23.7	36.9	16.7
0.9_60C_3d_Spot3	26.1	28.7	32.1	13.0	22.3	23.6	38.2	15.9
0.9_60C_3d_Spot4	24.9	28.2	32.8	14.0	21.1	23.0	38.8	17.0
0.9_60C_3d_Spot5	26.4	27.1	30.4	16.0	22.4	22.1	36.0	19.5

A.2 Si/Al = 3.0

TABLE A.2 – EDS spectrum of Si/Al = 3.0 pastes after 3 days of curing at 60°C.

Sample	At(%)				Wt(%)			
	Si	Al	K	Ca	Si	Al	K	Ca
3.0_60C_3d_Spot1	56.9	13.8	19.5	9.9	51.1	11.9	24.3	12.7
3.0_60C_3d_Spot2	59.1	13.4	18.1	9.4	53.5	11.6	22.7	12.1
3.0_60C_3d_Spot3	54.2	13.5	21.5	10.8	48.2	11.5	26.6	13.7
3.0_60C_3d_Spot4	56.3	13.6	19.8	10.3	50.4	11.7	24.7	13.2
3.0_60C_3d_Spot5	56.4	13.4	20.6	9.6	50.5	11.5	25.7	12.3
3.0_60C_3d_Spot6	56.6	12.5	20.8	10.1	50.6	10.8	25.8	12.9

A.3 Si/Al = 5.0

TABLE A.3 – EDS spectrum of Si/Al = 5.0 pastes after 3 days of curing at 60°C.

Sample	At(%)				Wt(%)			
	Si	Al	K	Ca	Si	Al	K	Ca
5.0_60C_3d_Spot1	59.5	9.2	19.6	11.6	53.0	7.9	24.2	14.9
5.0_60C_3d_Spot2	61.5	10.5	18.8	9.3	55.4	9.1	23.5	11.9
5.0_60C_3d_Spot3	58.3	8.9	20.8	12.0	51.7	7.6	25.7	15.0
5.0_60C_3d_Spot4	48.5	7.7	33.3	10.4	41.4	6.4	39.5	12.7
5.0_60C_3d_Spot5	51.1	8.3	32.8	7.8	44.9	6.8	39.5	9.7
5.0_60C_3d_Spot6	58.6	9.5	21.5	10.4	52.1	8.1	26.6	13.2

Annex A - Main solid precursors

This annex summarizes the characteristics of common materials that can be used as solid precursors in the production of more sustainable binders.

TABLE A.1 – Characteristics of common or innovative residual materials that can be added to concrete to produce more sustainable binders (NODEHI; TAGHVAEE, 2022).

Additive name	Usual form	Average density (kg/m^3)	Average particle size (µm)	Limitations	Benefits
Silica fume	Spherical	2200	0.1–0.5	Reduces workability and initial strength	Increases compactness, mechanical strength, and durability
GGBFS	Angular with rough surface	1000–1300	1.25–250	Low initial strength	Increases durability, improves ITZ, and sulfate resistance
Fly ash	Spherical	540–860	0.5–300	Low initial strength	Improves workability and long-term strength
Metakaolin	Porous, lamellar, and angular	890	1–20	Reduces workability	Fills microstructure and improves ITZ
Rice husk ash	Irregular with high porosity	504–700	5–10	Property variation and low reactivity	High silica content; improves compactness and strength
Glass powder	Irregular	2500	0.8–50	High contamination	Improves durability and pozzolanic reaction
Red mud	Irregular and needle-shaped	2700–3400	100 to over 200	High contamination	High alumina content, can improve hydration
Ceramic waste	Angular	1700	Below 100	–	Improves compactness and performance
MSWI	Irregular	660–1690	–	–	Improves microstructure and reduces porosity
Paper sludge ash	Irregular	Below 100	–	–	Favourably adjusts the S/A ratio

FOLHA DE REGISTRO DO DOCUMENTO

1. CLASSIFICAÇÃO/TIPO	2. DATA	3. DOCUMENTO Nº	4. Nº DE PÁGINAS
TC	12 de novembro de 2025	DCTA/ITA/TC-044/2025	57

5. TÍTULO E SUBTÍTULO:
Development of one-part alkali-activated cement with low-calcium solid precursors and alternative alkaline sources.

6. AUTOR(ES):
Felipe Mello dos Reis

7. INSTITUIÇÃO(ÕES)/ÓRGÃO(S) INTERNO(S)/DIVISÃO(ÕES):
Instituto Tecnológico de Aeronáutica – ITA

8. PALAVRAS-CHAVE SUGERIDAS PELO AUTOR:
AAM; Geopolymer; One-part.

9. PALAVRAS-CHAVE RESULTANTES DE INDEXAÇÃO:
Cimentos; Ligantes; Desenvlvimento sustentável; Concretos; Soluções alcalinas; Propriedades mecânica; Construção civil; Engenharia civil.

10. APRESENTAÇÃO: (**X**) **Nacional** ( ) **Internacional**
ITA, São José dos Campos. Curso de Graduação em Engenharia Civil-Aeronáutica. Orientador: Prof. Dr. João Cláudio Bassan de Moraes. Publicado em 2025.

11. RESUMO:
In the search for more sustainable alternatives to Portland cement, alkali-activated cements have been extensively studied. Initially, most mixing processes occur in two steps, which sacrifice productive efficiency in favor of improved mechanical properties. Aiming to increase process scalability, the development of one-part (just-add-water) systems has brought a more accessible and practical technology to the industry. Nonetheless, current studies mainly focus on calcium-rich precursors, while the use of conventional alkaline activators raises concerns related to safety and environmental impact. This work proposes the development of a one-part alkali-activated cement using low-calcium solid precursors, such as silica fume and metakaolin, along with safer and sustainable alkaline sources, such as potassium carbonate and calcium hydroxide. The variation of the Si/Al molar ratio directly influenced both the polymerization kinetics and microstructural characteristics of the binders. Mixtures with Si/Al = 3.0 achieved the best balance between density, porosity, and mechanical strength, reflecting an optimal degree of geopolymerization and homogeneous gel formation. Microstructural analyses confirmed the formation of predominantly amorphous aluminosilicate gels (K-A-S-H), with gel characteristics dependent on precursor proportions. The results demonstrated that the proposed formulation is technically viable, producing stable and compact matrices with adequate mechanical performance and improved safety and sustainability compared to conventional alkali-activated systems. The study demonstrates that combining metakaolin and silica fume with mild alkaline sources is a promising strategy for developing a binder with adequate mechanical performance and enhanced viability for application in the construction industry.

12. GRAU DE SIGILO:
(**X**) **OSTENSIVO** ( ) **RESERVADO** ( ) **SECRETO**